

THE LUMINOUS X-RAY SOURCE POPULATION IN M51 OBSERVED WITH *CHANDRA*YUICHI TERASHIMA<sup>1,2</sup> AND ANDREW S. WILSON<sup>1,3</sup>*Submitted to The Astrophysical Journal.*

## ABSTRACT

We present the results of two *Chandra* observations (separated by 1 year) of the population of X-ray sources in the spiral galaxy M51 (NGC 5194 and NGC 5195). 113 X-ray sources have been detected in an  $8\frac{1}{4} \times 8\frac{1}{4}$  ( $20.4 \times 20.4$  kpc) region, and 84 and 12 of them project within the disks of NGC 5194 and NGC 5195, respectively. Nine and 28 sources have luminosities exceeding  $1 \times 10^{39}$  ergs s<sup>-1</sup> (ultraluminous X-ray sources or ULXs) and  $1 \times 10^{38}$  ergs s<sup>-1</sup> in the 0.5 – 8 keV band, respectively, assuming they are associated with M51. The number of ULXs is much higher than found in most normal spiral and elliptical galaxies. Most of the X-ray sources and all seven of the ULXs in NGC 5194 are located in, or close to, a spiral arm, suggesting a connection with recent star formation. The cumulative luminosity function of the X-ray sources in NGC 5194 with  $L(0.5 - 8 \text{ keV}) > 10^{38}$  ergs s<sup>-1</sup> is well described by a power law  $N(> L(0.5 - 8 \text{ keV})) \propto L(0.5 - 8 \text{ keV})^{-\alpha}$  with  $\alpha = 0.91$ . The X-ray spectra of most of the detected sources are consistent with a power law with a photon index between 1 and 2, with a few sources showing harder or softer spectra. The spectra of most ULXs are consistent with both a power law and a multicolor disk blackbody (MCD) model, while a power law model is preferable to a MCD model in two ULXs. One ULX (NGC 5194 #69) shows drastic spectral steepening accompanied by a decline in luminosity by a factor of 3460 in the 2 – 10 keV band between the two observations. This source also exhibited a possible period of 2.1 hrs in the year 2000 observation. Another ULX (NGC 5194 #26) shows strong emission lines from highly ionized species. The masses of the compact objects and mass accretion rates in ULXs and other X-ray sources are not well constrained by these observations. If we adopt a MCD interpretation, their MCD parameters imply that most of the X-ray sources are stellar mass ( $\sim 5 - 10 M_{\odot}$ ) black holes accreting near or above the Eddington rate, although other possibilities (intermediate-mass black holes and relativistically beamed emission) cannot be excluded. The power law sources may, instead, represent Comptonized disk, or nonthermal, emission. Two ULXs have very soft spectra; MCD models require  $kT \approx 0.1$  keV. We discuss the possibility that this soft emission originates in an accretion disk around an intermediate-mass black hole. We also present a study of the nucleus of, and discrete sources (including two ULXs) in, the companion galaxy NGC 5195.

*Subject headings:* accretion, accretion disks — galaxies: active — X-rays: binaries — X-rays: galaxies — galaxies: Individual (M51)

## 1. INTRODUCTION

The X-ray emission from a galaxy consists of various components including discrete sources, such as X-ray binaries and supernova remnants, diffuse hot gas, and an active galactic nucleus (AGN), if present. One of the most intriguing and puzzling classes of X-ray source comprises the so called ultraluminous X-ray sources (ULXs), whose luminosities ( $> 10^{39}$  ergs s<sup>-1</sup>, sometimes  $> 10^{40}$  ergs s<sup>-1</sup>) considerably exceed the Eddington luminosity of a neutron star (e.g., Fabbiano 1996; Makishima et al. 2000 and references therein). An ULX may be a stellar mass black hole radiating near or above the Eddington luminosity (Begelman 2002), a stellar mass black hole or neutron star with beamed X-ray emission (Reynolds et al. 1997; King et al. 2001; Körding, Falcke, & Markoff 2002), or an intermediate mass ( $\sim 100 M_{\odot}$  or higher, but smaller than those in AGNs) black hole radiating near or lower than the Eddington luminosity (Matsumoto et al. 2001, Kaaret et al. 2001).

Since the launch of the *Chandra* X-ray observatory, which has unprecedented spatial resolution ( $\approx 0.5$  arcsec) as well as moderate spectral resolution over a broad band (0.1–10 keV), X-ray source populations and luminosity functions in nearby galaxies have been extensively studied. One pertinent finding is that starburst galaxies often contain ULXs (e.g., Kilgard et al.

2002 for a mini survey; M82: Matsumoto et al. 2001, Kaaret et al. 2001, Griffiths et al. 2000; the Antennae [NGC 4038/39]: Fabbiano, Zezas, & Murray 2001; the Circinus galaxy: Bauer et al. 2001, Smith & Wilson 2001; NGC 3256: Lira et al. 2002; NGC 3628: Strickland et al. 2001). This finding strongly suggests that many ULXs are associated with ongoing star formation, and perhaps with massive stars.

Studies of spectra and variability of ULXs are essential to understand their nature. Detection of time variability provides strong support for the hypothesis that the observed luminosity originates in a single source, not multiple sources. Investigations of spectral variability are important to pursue the origin of the X-ray emission. Flux and spectral variability has been reported for several ULXs (e.g., the Antennae, Fabbiano et al. 2003). For example, a soft/hard spectral transition has been observed in the two ULXs in the nearby galaxy IC 342 (Kubota et al. 2001a). Such behavior is reminiscent of Galactic black hole candidates and strongly favors an accreting black hole origin for these sources. If a black hole plus accretion disk interpretation of ULXs is correct, the variability of the source luminosity and the temperature and inner radius of the disk can be used to constrain the structure of an accretion disk radiating at near or above the Eddington rate (Mizuno et al. 2001; Watarai, Mizuno, & Mineshige 2001). If an accretion rate is high and a

<sup>1</sup> Astronomy Department, University of Maryland, College Park, MD 20742

<sup>2</sup> Institute of Space and Astronautical Science, 3-1-1 Yoshinodai, Sagami-hara, Kanagawa 229-8510, Japan

<sup>3</sup> Adjunct Astronomer, Space Telescope Science Institute, 3700 San Martin Drive, Baltimore, MD 21218

disk is geometrically thick, collimation (non-relativistic mild beaming) might be important (e.g., King et al. 2001, King 2002). Alternatively, the X-ray emission could originate in a disk corona or from a relativistic jet. The luminosity function of the X-ray sources and the environment in which the ULXs reside are also important clues to their origin (e.g., Zezas & Fabbiano 2002).

The nearby (8.4 Mpc; Feldmeier et al. 1997) spiral galaxy NGC 5194 and its companion NGC 5195 (together comprising M51) represent one of the best targets for studying a galactic X-ray source population, including ULXs. Previous observations with the *ROSAT* PSPC and HRI have revealed the presence of luminous X-ray sources, including 2–4 sources whose luminosities exceed  $10^{39}$  ergs  $s^{-1}$  (Marston et al. 1995; Ehle, Pietsch, & Beck 1995; Read, Ponman, & Strickland 1997; Roberts & Warwick 2000; Colbert & Ptak 2002). Additionally, since the galaxy is near face-on, absorption by gas in the galaxy disk is much less serious than in highly inclined systems. Furthermore, M51 fits nicely onto a single *Chandra* CCD, greatly simplifying the analysis of the X-ray source population.

In this paper, we present the properties of X-ray sources in NGC 5194 and NGC 5195 obtained with two *Chandra* observations separated by almost exactly a year. A *Chandra* study of the Seyfert 2 nucleus of NGC 5194 and its extended bi-polar X-ray lobes can be found in Terashima & Wilson (2001). For an assumed distance of 8.4 Mpc, 1 arcsec corresponds to 40.7 pc.

This paper is organized as follows. In section 2, observations and data reduction are presented. Section 3 is devoted to the source detection procedure, the source list and locations, variability, spectra, and the X-ray luminosity function. A discussion of the nature of the X-ray sources is given in section 4, and section 5 summarizes the results and conclusions.

## 2. OBSERVATION AND DATA REDUCTION

*Chandra* observations of M51 were performed on 2000 June 20 and 2001 June 23 with the ACIS instrument. The background was stable in both observations and effective exposure times of 14.9 ksec and 26.8 ksec were obtained for the observations in 2000 and 2001, respectively. The two observations were done with almost identical pointing. The offsets between the two pointing positions and roll angles were  $\approx 2$  arcsec and  $2^\circ 3'$ , respectively. The nucleus of NGC 5194 was placed at the aim point on the back-illuminated CCD S3 chip and almost all of NGC 5194 and NGC 5195 fall on this chip. In this paper, we use the S3 chip only. The data were processed by CIAO version 2.1 and CALDB version 2.7. Only *ASCA* (“good”) grades 0, 2, 3, 4, 6 were used in the analysis.

## 3. RESULTS

### 3.1. X-ray Image and Source Detection

A color image adaptively smoothed with the CIAO task “csmooth” is shown in Fig. 1. The three energy bands 0.3–1.5 keV, 1.5–3 keV, and 3–8 keV correspond to red, green, and blue, respectively. In this image, we see extended emission distributed over NGC 5194, a bright nuclear region (see also Terashima & Wilson 2001), and many discrete sources. The companion galaxy NGC 5195 also shows discrete sources and diffuse emission. The color indicates that the diffuse emission has a very soft spectrum, while the discrete sources show a range of spectral hardness. The spectra of the discrete sources are presented in section 3.4.

We used the “wavdetect” program in the CIAO package for detecting sources. The wavelet source detection threshold was set to be  $10^{-6}$ , which implies one or less false source would be detected on the entire S3 chip. Wavelet scales of 1,  $\sqrt{2}$ , 2,  $2\sqrt{2}$ , 4,  $4\sqrt{2}$ , 8,  $8\sqrt{2}$ , and 16 pixels were used (the pixel size of the ACIS corresponds to 0.49 arcsec). We ran wavdetect for three data sets: the observation in 2000, that in 2001, and the combined data of the two. The source searches were performed in the three energy bands 0.5–8 keV, 0.5–2 keV, and 2–8 keV. We refer to these three bands as full, soft, and hard, respectively. We thus obtained nine source lists, which were combined into one final source list. The source candidates in each list were carefully examined in the raw images by eye and we decided to include only sources with a significance greater than  $3\sigma$  in our source list and analysis. The nuclear region of NGC 5194, containing the Seyfert nucleus and associated outflows, is very bright in X-rays (see Terashima & Wilson 2001), so emission from within the rectangular region  $\alpha = 13^{\text{h}}29^{\text{m}}51^{\text{s}}9 - 53^{\text{s}}4$ ,  $\delta = 47^\circ 11'36'' - 56''$  (J2000) is excluded from all the tables presented in this paper. The counts obtained from “wavdetect” were compared with the results of manual photometry, in which extraction radii of 4–10 pixels were used, depending on the off axis angle of the source. Background counts were determined from the region surrounding the source, and nearby sources were excluded. The number of counts obtained from each source by manual photometry was usually in good agreement with that obtained by wavdetect. For a few sources, the measured counts disagreed with the number obtained by wavdetect. In such cases, we examined the images and decided to use the results of the manual photometry.

Some sources were detected in only one or two out of the three energy bands. We calculated upper limits to the counts in the undetected band(s) at 95% confidence level by interpolating between the values in Table 2 of Kraft, Burrows, & Nousek (1991). A source detected in only one or two out of the three data sets (observations 1, 2, and 1+2 combined) was treated in a similar way. Upper limits to the counts in the source region and counts in the surrounding background region were determined by manual photometry using the same procedure as used above.

The numbers of sources detected in each energy band and each data set after this screening are summarized in Table 1. 113 sources are detected on the entire S3 chip. The source locations were compared with an optical image (Thilker et al. 2000). Sources within  $200''$  of the nucleus of NGC 5194 are assumed coincident with NGC 5194 and those within  $75''$  of the nucleus of NGC 5195 are taken to be coincident with NGC 5195 (Tables 2 and 3, respectively). Other sources detected on the S3 chip are shown in Table 4. In these tables we give: the source identification number used in this paper (column 1), right ascension (column 2), declination (column 3), *Chandra* source name (column 4), observed counts in the full, soft, and hard bands for the combined data set of the first and second observations (columns 5–7), observed counts in the first observation (columns 8–10), and observed counts in the second observation (columns 11–13). The number of counts in these tables is not corrected for vignetting and the quoted errors on the counts represent the  $1\sigma$  range. The brightest source is CXOM51 J133007.6+471106 in the first observation (0.055 counts  $s^{-1}$  in the 0.5–8 keV band). The pile up fraction is a few percent for this source. Therefore, pile up is negligible for all sources.

The X-ray position of the Seyfert nucleus ( $13^{\text{h}}29^{\text{m}}52^{\text{s}}72$ ,  $47^\circ 11'42.''7$ )

(J2000) is in good agreement with the position of the radio nucleus ( $13^{\text{h}}29^{\text{m}}52^{\text{s}}.7101 \pm 0^{\text{s}}.0016, 47^{\circ}11'42''.696 \pm 0''.026$  (J2000)) measured with the VLA in A-configuration at 8.4 GHz, Kaiser et al. 2001). The source CXOM51 J132938.6+471336 is also in agreement with the position of a star. Therefore, we did not make any corrections to the source positions.

The detection limit is about seven counts in each observation, which corresponds to  $3.9 \times 10^{-15}$ ,  $2.2 \times 10^{-15}$ , and  $1.4 \times 10^{-15}$  ergs  $\text{s}^{-1} \text{cm}^{-2}$ , for the first observation, the second observation, and the sum of the first and second observations, respectively, in the 0.5–8 keV band for a typical spectrum (a power law with a photon index of 1.5 absorbed by the Galactic column  $N_{\text{H}} = 1.3 \times 10^{20} \text{ cm}^{-2}$  (Stark et al. 1992)). According to the  $\log N - \log S$  relation from the *Chandra* deep surveys (Mushotzky et al. 2000; Tozzi et al. 2001; Brandt et al. 2001), the expected number of background sources is 8–12 on the entire S3 chip above the flux limit for the sum of the two observations, where the effects of vignetting and bad pixels have been taken into account to calculate our survey area. Since the detected number (17) of sources listed as outside NGC 5194 and NGC 5195 (Table 4) is larger than that expected for background sources (4–6), some of the sources shown in Table 4 are apparently associated with M51.

### 3.2. Source Locations

#### 3.2.1. Comparison with ROSAT Sources

We have compared our source list with previous X-ray observations. The best X-ray source list before *Chandra* was obtained with *ROSAT* (Ehle, Pietsch, & Beck 1995 (HRI); Marston et al. 1995 (PSPC); Roberts and Warwick 2000 (HRI); Read, Ponman, & Strickland 1997 (PSPC); Colbert & Ptak 2002 (HRI)). Correspondences between *Chandra* and *ROSAT* sources are given in Table 5, where we list all the *ROSAT* sources within  $12''$  of a given *Chandra* source (the *ROSAT* positions have uncertainties of  $\approx 10''$ ).

Four *ROSAT* sources have two *Chandra* counterparts in their error circles (NGC 5194 *Chandra* #5 and 6, # 27 and 28, #41 and 42, and # 69 and 70). This result demonstrates that luminous X-ray sources found with low-spatial resolution can be superpositions of two or more sources and that interpretation should be made with caution. One *ROSAT* source (source 7 in Ehle et al. = source 4 in Marston et al. = source 4 in Read et al.) has no *Chandra* counterpart. The *Chandra* counterparts of two *ROSAT* sources (source 5 in Marston et al. = source 3 in Read et al., and source 6 in Ehle et al. = source 3 in Roberts & Warwick) are very faint (9 counts and 29 counts, respectively, in the 0.5–8 keV band for the total of the two *Chandra* observations). The first (*Chandra* #16) is almost at the detection limit of *Chandra*. These *ROSAT* sources with no or a very faint *Chandra* counterpart, indicating drastic flux decreases from the *ROSAT* to the *Chandra* observations, are likely to be transient sources.

The brightest source (CXOM51 J133007.6+471106 = NGC 5194#82) may be identified with a source detected in an *Einstein* HRI image (Palumbo et al. 1985) and a *BeppoSAX* image (Fukazawa et al. 2001).

#### 3.2.2. Optical Counterparts

In Fig. 2, the positions of the detected sources are overlaid on a narrow-band optical image including  $\text{H}\alpha$  and the nearby continuum (Thilker et al. 2000). Most of the discrete sources in

NGC 5194 are located in or near the spiral arms, but sources are also found between the arms. A few X-ray sources appear to be associated with bright H II regions, while others show no clear association with optical sources. All 7 of the ULXs in NGC 5194 are in, or close to, a spiral arm, supporting an association between ULXs and star formation.

We cross-correlated the X-ray source positions with the list of H II regions in NGC 5194 obtained by Thilker et al. (2000). Among the 1625 H II regions in their catalog above a  $5\sigma$  detection limit of  $L_{\text{H}\alpha} = 10^{36}$  ergs  $\text{s}^{-1}$ , about 1350 fall on *Chandra* chip S3. We found that 22 of these 1350 H II regions have an X-ray source within  $1.5''$  or 61 pc. Most of the 22 H II regions are very faint, and only two bright H II regions have a candidate X-ray counterpart (NGC 5194 #55 = CXOM51 J132955.5+471402 and NGC 5194 #59 = CXOM51 J132955.9+471145). These two X-ray sources are faint in X-rays (17 and 43 counts, respectively, were detected in the 0.5–8 keV band in the sum of the two observations).

Four (NGC 5194 #37 = CXOM51 J132953.3+471042, NGC 5194 #41 = CXOM51 J132953.7+471436, NGC 5194 #69 = CXOM51 J133001.0+471344, NGC 5194 #82 = CXOM51 J133007.6+471106) out of the seven ULXs have an extremely faint H II region, which is not visible in Fig 2, within  $1''.5$ . One ULX (NGC 5194 #26 = CXOM51 J132950.7+471155) is  $2''.3$  away from an H II region and is in a chain of bright H II regions along an inner spiral arm.

30 point sources have been detected in multi-band *HST* WFPC2 images of the central ( $11'' \times 16''$ , or  $450 \times 650$  pc) region (Table 2 in Lamers et al. 2002). Lamers et al. (2002) argue that most of these point sources are isolated massive stars, rather than clusters. Unfortunately, most of these sources are located in the region of the bright, nuclear, diffuse X-ray emission, which probably originates from gas heated by the jets from the AGN (Terashima & Wilson 2001), and no X-ray point sources are seen at the positions of the *HST* sources. A few *HST* sources are outside the diffuse X-ray emission but we find no X-ray counterparts.

Globular clusters appear to be the dominant sites of luminous low mass X-ray binaries in early-type galaxies (Angelini et al. 2001; Kundu et al. 2002; Di Stefano et al. 2003). However, the fraction of the unresolved X-ray sources in the spirals M81 (Swartz et al. 2003) and M31 (Kong et al. 2002) that are associated with known globular clusters is small. Unfortunately, we cannot evaluate the association between compact X-ray sources and globular clusters in M51 as we are unaware of any catalog of globular clusters in this galaxy.

#### 3.2.3. Radio Counterparts

We searched for counterparts in a FIRST VLA survey image at 1.4 GHz and in the source list from VLA 6 and 20 cm observations by Ho & Ulvestad (2001; their Table 4) and found no radio counterparts, except for the nuclei of NGC 5194 and NGC 5195.

### 3.3. Variability of Point Sources

#### 3.3.1. Short-term Variability

We have searched for short-term variability of relatively bright point sources by investigating their fluxes within each observation. There are 16 and 22 sources with  $> 70$  counts per observation in the 0.5–8 keV band in the first and second observation, respectively. Light curves with a time bin of 2000

sec were created and examined with the Kolmogorov-Smirnov (K-S) test to evaluate the null hypothesis that any given source has constant flux.

In the first observation, NGC 5194 #63 (= CXOM51 J132957.6+471048) shows a low KS probability ( $2 \times 10^{-7}$ ) (Fig. 3a). Another object (NGC 5194 #69 = CXOM51 J133001.0+471344) shows two peaks separated by  $\approx 7000$  sec (Fig. 3b), which may be a periodicity or two physically distinct flux peaks. Liu et al. (2002) interpreted these features as indicating a 2.1 hr period, although only two periods are covered by the observation.

In the second observation, one source (NGC 5194 #76 = CXOM51 J133004.3+471321) clearly shows a declining flux, going nearly to zero in the second half of the observation. The light curve of this object is shown in Fig. 3c. The light curves of other sources have KS probabilities greater than  $1 \times 10^{-4}$  and variability is not significant. NGC 5194 #69 was very dim (46 counts detected in 0.5–8 keV) in the second observation, and the variability seen in the first observation is not detected.

### 3.3.2. Long-term Variability

We compared the count rates obtained in the two separate observations as a means of searching for variability on a time scale of a year. Fig. 4 shows the ratio of the count rate,  $C(0.5\text{--}8\text{ keV})$ , in the second observation to that in the first observation plotted against the luminosity in the 0.5–8 keV band for the sources in NGC 5194 and NGC 5195. The luminosities were calculated from the total counts of the two observations, assuming a power-law spectrum with a photon index derived from the band ratio,  $C(2\text{--}8\text{ keV})/C(0.5\text{--}2\text{ keV})$ , and absorption by only the Galactic column. When only an upper or lower limit on the band ratio is available, the typical photon index of 1.5 was assumed if the band ratio is consistent with this value; otherwise we used the limit on the band ratio to estimate the spectral shape. The numbers of objects in NGC 5194 which show time variability at greater than the  $3\sigma$  level in the full, soft, hard, and any one of these three bands are shown in Table 1. About one-third of discrete sources in NGC 5194 exhibit time variability, which strongly implies that these sources are single (or at most a few) compact objects, and are most likely to be black hole binaries powered by accretion, given their large luminosities ( $\gtrsim 10^{38}$  ergs  $s^{-1}$ ). Their band ratios and spectra are also consistent with an X-ray binary interpretation (section 3.4), except for a few cases. A small fraction could be recent supernovae, which show variability on a timescale of  $\sim 1$  yr (e.g., Immler & Lewin 2002).

Four objects show large amplitude variability (a factor of ten or more), suggesting a transient nature. Two of them are ULXs, demonstrating that there are two classes of these objects, i.e., transient and persistent ULXs.

## 3.4. X-ray Spectra of Point Sources

### 3.4.1. Spectra of Bright Point Sources

Spectral fits were performed for sources with  $>70$  detected counts in the 0.5–8 keV band in one observation using XSPEC version 11. In all, spectral models were obtained for 38 spectra of 26 sources. The spectra were grouped so that each spectral bin contained at least 15 counts, and the  $\chi^2$  minimization technique was employed in the fit unless otherwise noted. We obtained a background spectrum for each source from an adjacent field and subtracted the background from the source spectrum. Any sources in the background region were excluded.

Two models — a power law and a multicolor disk blackbody (MCD, Mitsuda et al. 1984, Makishima et al. 1986) — were examined in spectral fitting. In some cases, these models did not provide satisfactory representations of the data and other models were examined, as discussed below. The results of the spectral modeling are summarized in Tables 6 and 7 for objects with luminosities in the 0.5–8 keV band greater than and less than  $10^{39}$  ergs  $s^{-1}$ , respectively. Note that a given source may have  $L(0.5\text{--}8\text{ keV}) > 10^{39}$  ergs  $s^{-1}$  in one observation or when modeled with a particular choice of spectrum, and  $L(0.5\text{--}8\text{ keV}) < 10^{39}$  ergs  $s^{-1}$  otherwise. The errors or parameter ranges shown in this paper represent the 90% confidence level for one parameter of interest ( $\Delta\chi^2 = 2.7$ ) unless otherwise stated. Luminosities for a MCD model are calculated by assuming the inclination of the disk  $i = 60^\circ$ , i.e.,  $L = 2\pi D^2 F(\cos i)^{-1} = 4\pi D^2 F$ , where  $F$  is the observed flux and  $D$  is the distance. Errors, fluxes, and luminosities are not shown for unacceptable fits.

### 3.4.2. Band ratios

Figs. 5a and 5b show the dependence of the band ratio on counts in the 0.5–8 keV band for sources in NGC 5194 and NGC 5195, respectively; the summed data of the two observations are used. The counts are as observed and not corrected for the effects of vignetting and the edge of the CCD chip. The band ratios for power law spectra modified by Galactic absorption are shown as dashed lines for photon indices of  $-1.0, 0.0, 1.0, 2.0,$  and  $3.0$ . We calculated the source luminosities as described in section 3.3.2. The dependence of the band ratio on luminosity is displayed in Figs. 6a and 6b for NGC 5194 and NGC 5195, respectively. These plots show that most of the relatively luminous ( $> 10^{38}$  ergs  $s^{-1}$ ) sources have spectra consistent with a power law with a photon index between 1 and 2, while some sources have very flat or steep spectra. There is no obvious dependence of photon index on luminosity.

## 3.5. Luminosity Function

Using the luminosities derived earlier (from the total counts in the two observations - section 3.3.2), we have calculated the cumulative luminosity function in the 0.5 - 8 keV band for the X-ray sources in NGC 5194 (Fig. 7). The luminosity function was modelled as a power law function above  $10^{38}$  ergs  $s^{-1}$ , where it is virtually free from incompleteness. We confirmed that incompleteness is negligible above  $10^{38}$  ergs  $s^{-1}$  by comparing our source and background counts with the simulations presented in Kim & Fabbiano (2003). We used a maximum-likelihood method and calculated errors by means of the Gehrels approximation (Gehrels 1986). A power-law slope of  $\alpha = 0.91 \pm 0.14$  ( $N(> L(0.5\text{--}8\text{ keV})) \propto L(0.5\text{--}8\text{ keV})^{-\alpha}$ ) was obtained. The luminosity function does not require a break around the Eddington luminosity for  $1.4M_\odot$ , as has been found in several early type galaxies (Sarazin, Irwin, & Bregman 2000; Blanton, Sarzin, & Irwin 2001; Irwin, Sarazin, & Bregman 2002).

In the model fit, the errors in the number of sources in each bin were taken into account while other sources of error, such as uncertainties in photon count rates and spectral shapes, were ignored. These latter effects are, however, relatively small since we discarded the low luminosity ( $< 10^{38}$  ergs  $s^{-1}$ ) sources, of which there are many but the photon statistics for each source are poor (e.g., Zezas & Fabbiano 2002).

#### 4. DISCUSSION

##### 4.1. Incidence of Ultra Luminous X-ray Sources and Luminosity Function of X-ray Sources

Our observations have detected many luminous sources, among which 7 and 28 sources in NGC 5194 have a luminosity (0.5–8 keV) greater than  $10^{39}$  and  $10^{38}$  ergs  $s^{-1}$ , respectively, assuming they are associated with M51. Two source in NGC 5195 has a luminosity in excess of  $10^{39}$  ergs  $s^{-1}$ . The number of ULXs, defined as  $L(0.5-8 \text{ keV}) > 10^{39}$  ergs  $s^{-1}$ , is much higher than typically seen in spiral galaxies (0–2; e.g., Roberts & Warwick 2000). The large number of luminous X-ray sources is not simply related to the number of young stars in M51. In fact, the absolute B magnitude, which is often used as a measure of the relatively young stellar population, of NGC 5194 is modest ( $M_{B_T}^0 = -20.95$ , calculated from information in the RC3 catalog for our assumed distance) in comparison with the other spiral galaxies studied by Roberts & Warwick (2000). Indeed, the majority of galaxies with similar values of  $M_B$  to M51 possess no ULXs.

NGC 5194 is a classical, nearby Sc galaxy. It thus has star formation associated with density-wave driven spiral arms in an ISM rich in molecular gas (e.g., Scoville et al. 2001). Most of the detected X-ray sources are located in or near the spiral arms (Fig. 2). Further, all 7 of the ULXs in NGC 5194 are in, or very close to, a spiral arm. Our results thus confirm that the ULXs in M51 are associated with star formation, but in a different context to starburst galaxies, such as NGC 1068 (a very luminous circumnuclear disk starburst possibly related to the AGN; see Smith & Wilson [2003] for the X-ray source population) and interacting galaxies, such as the Antennae (galaxy merger-driven star formation; see Zezas & Fabbiano [2002] for the X-ray source population).

As noted in section 3.5, the cumulative luminosity function for the X-ray sources in NGC 5194 is well fitted by a power law with a slope of 0.91 above  $10^{38}$  ergs  $s^{-1}$  (Fig. 7). This slope is inbetween the values found in disk galaxies (1.1–1.4) and active starforming galaxies (0.5–0.8 for M82, NGC 253, and the Antennae), and significantly lower than those derived for ellipticals and lenticulars (Kilgard et al. 2002 and references therein). A break in the luminosity function (i.e. a change in its slope) can potentially be used to measure the formation history and age of the X-ray source population (Kilgard et al. 2002, Wu et al. 2003) and the amount of beaming in luminous sources (Körding et al. 2002). Such a break is not apparent in the luminosity function of NGC 5194. A power-law shape without a break is in agreement with luminosity functions observed for X-ray sources in starburst galaxies and in the galaxy disk of M81 (Tennant et al. 2001, Swartz et al. 2003), and is indicative of on-going star formation (Wu et al. 2003).

##### 4.2. Spectra and Variability of Luminous and Ultra-luminous X-ray Sources

We have modelled the X-ray spectra of bright sources with two continuum models – a power law and a MCD (Tables 6 and 7). In this subsection, we discuss interpretations of the spectra and their variability in ULXs.

###### 4.2.1. ULXs with a Power Law Spectrum

The spectra of NGC 5194 #37 = CXOM51 J132953.3+471042 and NGC 5194 #82 = CXOM51 J133007.6+471106 (Fig. 8) in the second observation (June 2001) are better fitted with a

power law than a MCD model (Table 6). The ASCA spectra of ULXs studied by Makishima et al. (2000) are better modeled by a MCD than a power law. However, ULXs whose spectra are best fitted by a power law have been found in recent observations (e.g., a source in Holmberg II observed with ASCA [Miyaji, Lehmann, & Hasinger 2001]; sources in IC 342 observed with ASCA [Kubota et al. 2001a]; a source in NGC 3628 observed with *Chandra* [Strickland et al. 2001]; a source in NGC 4565 observed with *XMM-Newton* (RXJ 1236.2+2558 = XMM J123617.5+285855 = CXO J123617.4+255856 [Foschini et al. 2002]; NGC 5204 X-1 [Roberts et al. 2001]; several of the luminous sources in NGC 1068 observed with *Chandra* [Smith & Wilson 2003]). Thus it appears that the two sources in NGC 5194, along with these objects, constitute a class of ULXs whose spectrum is best described by a power law.

A power law spectrum may arise in several scenarios. Phenomenologically, a power-law like spectrum is found in the low/hard state or very high state of a black hole binary (e.g., Tanaka 1996, Done 2002). Physically, power law spectra may result from non-thermal, possibly relativistically beamed, X-ray emission from jets, as in blazars (Körding, Falcke, & Markoff 2002), or through Comptonization of photons from the accretion disk, as is believed to occur in the low/hard state and the very high state of a binary containing a black hole (Done 2002; Kubota, Done, & Makishima 2002).

If the power-law spectra are analogous to the low/hard state in Galactic black hole candidates and the state transition is governed by the mass accretion rate, the ULXs would be emitting at less than a few % of  $L_{\text{Edd}}$  (e.g., Done 2002). If this is the case, a very high mass ( $>$  a few times  $100 M_{\odot}$ ) black hole is required. It is, however, not clear that such an extrapolation from stellar mass to such high mass black holes is valid.

On the other hand, if the observed X-ray emission is significantly beamed toward us, the intrinsic luminosity would be much lower than we have derived by assuming isotropic radiation. In this case, basic quantities such as the mass of the compact object, mass accretion rate, and beaming factor cannot be obtained from the present data.

Alternatively, spectra which are good approximations to power law shapes may be the results of Comptonization of thermal emission from an accretion disk with a high accretion rate. Such strong Comptonization is believed to occur in Galactic jet sources (e.g., GRO J1655-40, Kubota, Makishima & Ebisawa 2001b) and possibly an ULX in IC 342 (Kubota et al. 2002). Kubota et al. (2002) reanalyzed the ASCA spectrum of source 1 in IC 342 observed in 2000. The spectrum can be fitted with either a power law ( $\Gamma = 1.73 \pm 0.06$ , modified by an ionized Fe-K edge at  $8.4 \pm 0.3$  keV) or a Comptonized blackbody with an inner disk temperature of  $kT_{\text{in}} = 1.1 \pm 0.3$  keV. Kubota et al. (2002) argued that the latter model is a more appropriate interpretation of the apparent power law shape observed in this source based on their detailed spectral analysis and the analogy with the spectral variability and Comptonization in Galactic jet sources. This type of spectral state was observed in GRO J1655-40 and XTE J1550-564 when the bolometric luminosity of the disk was around  $\sim 10$ -20% of its Eddington luminosity (Kubota et al. 2001b; Kubota 2001). In their analysis, the bolometric luminosity is calculated from the MCD parameters of the underlying disk emission (see section 4.2.5). If the bolometric luminosities of the two sources in NGC 5194 with power law spectra correspond to this Eddington ratio ( $L_{\text{bol}}/L_{\text{Edd}} = 0.1$ ), the masses of the compact object are  $>$

98  $M_{\odot}$  (source 37) and  $> 120 M_{\odot}$  (source 82 in 2001) taking  $L_{\text{Edd}} = 1.5 \times 10^{38}$  (M/ $M_{\odot}$ ) ergs  $\text{s}^{-1}$  (assuming spherical symmetry and a hydrogen to helium composition ratio of 0.76:0.23 by weight [e.g., Makishima et al. 2000]). However, it is not clear that such spectral behavior *always* appears at such an Eddington ratio. If the power-law state appears between the optically thick geometrically thin disk and the slim disk,  $L_{\text{bol}}/L_{\text{Edd}}$  would be 1–2. In this case, the masses are estimated to be  $> 5 M_{\odot}$  (source 37) and  $> 6 M_{\odot}$  (source 82 in 2001).

NGC 5194 #37 is detected in only the second observation, indicating the photon flux increased by a factor of 100 in the 0.5–8 keV band. Although this large variability may imply that the source is a transient X-ray binary, such behavior is also consistent with any of the possibilities described above.

On the other hand, NGC 5194 #82 is detected, and spectral information is available, in both observations. The spectrum flattened ( $\Gamma = 2.26$  to 1.86) and the flux decreased (by 40%) from the first to the second observation. This trend is consistent with that of Galactic BHCs in the low/hard state and in the state with strong Comptonization. In both states, steeper spectra are seen in higher flux states.

Thus, no strong constraints on the masses of the compact objects and mass accretion rates in these ULXs can be obtained. Future observations of spectral variability should be able to quantify the changes in spectral state, and hopefully allow fundamental parameters, such as black hole mass and mass accretion rate, to be determined.

#### 4.2.2. Spectral Steepening in NGC 5194 #69

NGC 5194 #69 = CXOM51 J133001.0+471344 shows remarkable spectral variability (Fig. 9). The photon flux in the 2–8 keV band decreased by a factor of more than 13 from the year 2000 to the year 2001 observation. The first spectrum is relatively hard:  $\Gamma = 1.24^{+0.12}_{-0.17}$  (power law) or  $kT_{\text{in}} = 2.3^{+1.0}_{-0.5}$  keV (MCD), while the second spectrum is extremely soft:  $\Gamma > 5.1$  (power law),  $kT_{\text{in}} = 0.17^{+0.13}_{-0.06}$  keV (MCD), or  $kT = 0.16^{+0.08}_{-0.06}$  keV (black body) (Table 6). The absorbing column increased from  $3.4^{+3.9}_{-3.4} \times 10^{20}$   $\text{cm}^{-2}$  to  $8.2^{+8.0}_{-5.0} \times 10^{21}$   $\text{cm}^{-2}$  from year 2000 to 2001 (values are for MCD models — Table 6). Our results are in general agreement with those of Liu et al. (2002), who analyzed the same observations. If we adopt a power law model and a MCD model for the first and second spectra, respectively, the intrinsic luminosity of this source declined by a factor of 3460 in the 2–10 keV band (the precise factor depends on the choice of spectral model). This object is the first example of such a drastic spectral change in ULXs, and is potentially extremely important for elucidating their true nature.

Such drastic steepening of the spectrum accompanied by a large flux decline is seen in soft X-ray transients. Soft X-ray transients show very soft spectra ( $kT = 0.2$ – $0.3$  keV for a black body model) when the luminosity goes below  $10^{34}$  ergs  $\text{s}^{-1}$  (Tanaka 1996, Tanaka & Shibazaki 1996). Such luminosities, however, are much lower than we observe in source NGC 5194 #69 in the second observation ( $5.6 \times 10^{38}$  ergs  $\text{s}^{-1}$  in 0.5–8 keV and  $7.4 \times 10^{35}$  ergs  $\text{s}^{-1}$  in 2–10 keV, the latter measured by extrapolating the best-fit MCD model up to 10 keV). For  $L(2$ – $10$  keV)  $\approx 6 \times 10^{35}$  ergs  $\text{s}^{-1}$ , Galactic black hole candidates are in a low/hard state, with spectra described by a power law with a photon index of 1.4–1.9, quite different to source #69 in 2001. Thus, it is not clear whether the similarity between the spectral shapes of the quiescent state of soft X-ray transients and NGC 5194 source # 69 in the second observation has any phys-

ical significance. If the transition of the spectra is governed by the mass accretion rate, observations of a state transition can be used as a measure of the mass of the central object and the mass accretion rate. The luminosity of NGC 5194 #69 in the state showing the very soft spectrum is more than 70 times higher than that of the similar state in stellar-mass black holes. If a simple scaling with mass is applied, the mass of the compact object in NGC 5194 #69 is  $\gtrsim 70$  times larger, i.e.  $\gtrsim$  several times  $100 M_{\odot}$ , which is in the range of intermediate-mass black holes (IMBHs). An improved understanding of the behavior of soft X-ray transients in our Galaxy, and monitoring of extragalactic luminous X-ray sources, will be crucial to pursue the true nature of luminous transient sources. Future observations of NGC 5194 # 69 are needed to confirm the possible periodicity of 2.1 hrs (see Fig. 3b); possible interpretations were discussed by Liu et al. (2002).

#### 4.2.3. Emission Lines in CXOM51 J 132950.7+471155 = NGC 5194 #26

CXOM51 J 132950.7+471155 = NGC 5194 #26 has the largest band ratio of all detected sources in M51 (Figs. 5a and 6a). This source can be seen as a blue (= very hard) source to the NW of the nucleus in the color image shown as Fig. 1 in Terashima & Wilson (2001).

This source shows a remarkable spectrum and variability. As shown below, the spectrum includes emission lines, and we use a spectrum with a finer-bin size to bring out these features. In the spectral fits, we adopted a maximum likelihood method using the C-statistic (Cash 1979), instead of  $\chi^2$  minimization, since each bin contains a small number ( $> 3$ ) of counts.

In the first observation (June 2000, Fig. 10a), the spectrum is quite hard and virtually no photons are detected in the low energy region below 1.5 keV. Since there are indications of emission lines, we added Gaussians to an absorbed power law continuum to model the spectrum. The results are summarized in Table 8, which includes identifications for the lines, assuming they are  $K\alpha$  transitions. The intrinsic luminosity corrected for absorption is  $3.4 \times 10^{39}$  ergs  $\text{s}^{-1}$  in the 0.5–8 keV band. We examined the statistical significance of these emission lines by Monte Carlo simulations. We simulated 2000 spectra with the best-fit continuum model and no emission lines, and fitted them with a model consisting of an absorbed power law and a Gaussian line. The line center energy was fixed at one of the four energies (1.8, 3.2, 4.0, and 6.7 keV) reported in Table 8. The width was fixed at 0. We calculated the probability that a fake line stronger than the actual data (Table 8) would be detected and obtained 4.0, 0.10, 0.15, and 0.40% for the lines at 1.8, 3.2, 4.0, and 6.7 keV, respectively. Thus the detection of these lines is highly significant.

On the other hand, emission-line features are not clearly seen in the spectrum obtained in the second observation (June 2001, Fig. 10b). In this case, the continuum is modeled as a partially-covered power law, and the spectral parameters are shown in Table 8. The intrinsic luminosity in the second observation ( $5.0 \times 10^{39}$  ergs  $\text{s}^{-1}$  in the 0.5–8 keV band) is 50% higher than that in the first observation.

Emission lines from highly ionized atoms and with large equivalent widths are observed in eclipses of high-mass X-ray binaries, when the direct emission from the compact object is blocked by the companion star, and only emission from and scattered by the photoionized medium surrounding the system (such as a stellar wind from the companion) is observed (e.g.,

Nagase et al. 1994; Ebisawa et al. 1996; Sako et al. 1999; Schulz et al. 2002). In such a situation, the intrinsic luminosity would be much larger (typically by a factor of 10–100; e.g., Nagase et al. 1994; Ebisawa et al. 1996) than the observed luminosity. If so, the observed luminosity implies that the intrinsic luminosity is at least  $\sim 5 \times 10^{40}$  ergs  $s^{-1}$  if the emission is isotropic. If this is the case, this system would be an eclipsing ULX. The spectrum in the second observation no longer shows strong emission lines, which implies that the contribution of direct emission from the compact object is significant. The observed luminosity in the second observation ( $5.0 \times 10^{39}$  ergs  $s^{-1}$  in 0.5–8 keV), however, is much lower than the expectation from the scattering picture ( $> 5 \times 10^{40}$  ergs  $s^{-1}$ ). Therefore, we conclude that an eclipse plus scattering scenario, with an isotropic X-ray source, is unlikely to account for the spectrum observed in June 2000.

The above luminosity problem could be resolved if the irradiating emission is anisotropic and beamed towards the scattering medium.

#### 4.2.4. Spectra and Variability of Other ULXs

The spectra of the two ULXs NGC 5194 #5 = CXOM51 J132939.5+471244 (Fig. 11a) and NGC 5194 #41 = CXOM51 J132953.7+471436 (Fig. 11b) can each be represented by either a power law or a MCD model (Table 6). The luminosity of the former source decreased by a factor of  $\approx 2.5$ , while that of the latter remained the same between the two observations. Although the best-fit spectral parameters of both these sources suggest that both spectra flattened, the errors are large and variability of the spectral shape is not statistically significant. The spectra of the source NGC 5195 #12 = CXOM51 J133006.0+471542 may also be described by either a power law or a MCD model; there is no evidence for variability.

#### 4.2.5. Multi Color Disk Blackbody Interpretation of the Spectra

The X-ray sources with  $10^{38} < L(0.5 - 8 \text{ keV}) < 10^{39}$  ergs  $s^{-1}$  are of significant interest since they could be a population intermediate between ULXs and ordinary X-ray binaries. The spectra of most of the sources in this luminosity range for which we performed spectral fitting (Table 7) may be described by either a power law or a MCD model.

If a power law is the correct description of the spectra of the two ULXs discussed in section 4.2.1 and the objects with  $L(0.5 - 8 \text{ keV}) < 10^{39}$  ergs  $s^{-1}$ , the same possibilities as described in section 4.2.1 are viable. Here, we examine the implications of an alternative interpretation of the spectra — MCD emission arising from optically thick accretion disks.

According to the MCD formalism of the spectrum from an optically-thick geometrically-thin accretion disk, the inner temperature of the disk  $kT_{\text{in}}$  depends on the mass accretion rate and black hole mass as  $kT_{\text{in}} \propto \eta^{1/4} M^{-1/4}$  (e.g., eq. (12) in Makishima et al. 2000), where  $\eta$  is the Eddington ratio ( $L_{\text{bol}}/L_{\text{Edd}}$ ) and  $M$  is the black hole mass. Fig. 12 shows the relation between the bolometric luminosity ( $L_{\text{bol}}$ ) and inner disk temperature  $kT_{\text{in}}$ . The expected relationships between  $L_{\text{bol}}$  and  $kT_{\text{in}}$  for a thin accretion disk with fixed black hole masses ( $M = 3, 6, 12,$  and  $24 M_{\odot}$ ) and fixed Eddington ratios ( $\eta = 0.01, 0.1, 1,$  and  $10$ ) are shown as dot-dashed and dashed lines, respectively. We have assumed that the disk inner radius,  $R_{\text{in}}$ , is equal to three Schwarzschild radii ( $R_S$ ), the ratio of the color temperature to the effective temperature (“spectral hardening factor”)  $\kappa = 1.7$

(Shimura & Takahara 1995), and the factor  $\xi$ , which corrects for the fact that  $T_{\text{in}}$  occurs at a radius somewhat larger than  $R_{\text{in}}$ , is  $\xi = 0.41$  (Kubota et al. 1998). The bolometric luminosity is calculated from  $L_{\text{bol}} = 4\pi(R_{\text{in}}/\xi)^2 \sigma(T_{\text{in}}/\kappa)^4$ . This plot is the same diagram as Fig. 3 in Makishima et al. (2000).

For each source, we calculated  $L_{\text{bol}}$  from the MCD model. The majority of the sources with  $L_{\text{bol}} \gtrsim 10^{39}$  ergs  $s^{-1}$  have the best-fit  $kT_{\text{in}}$  in the range 1.6–2.3 keV which is similar to the ULXs studied by Makishima et al. (2000) and higher than Galactic black hole candidates. The objects with  $L_{\text{bol}} = (5 - 10) \times 10^{38}$  ergs  $s^{-1}$  are clustered around  $\eta = 1$ . In other words, their temperature is comparable to that expected from the black hole mass determined by assuming that  $L_{\text{bol}} \approx L_{\text{Edd}}$  and their inferred masses are in the range of stellar-mass black holes ( $\sim 10 M_{\odot}$  or less). Three sources have relatively low temperatures ( $kT \approx 0.5$  keV) and small values of  $\eta$  ( $< 0.1$ ). The data suggest a correlation between  $L_{\text{bol}}$  and  $kT_{\text{in}}$ .

We note that X-ray spectra of Galactic BHCs in the high/soft state show a power law component in addition to the MCD component. If this power law component exists in the luminous sources, a MCD model might be too simplistic and lead to unphysical parameters. In BHCs, the MCD component dominates the X-ray spectrum below  $\sim 3$  keV, while the power law component is significant above several keV (e.g. Dotani et al. 1997), where the effective area of *Chandra* decreases. Therefore, the spectra obtained in the present work may not be sensitive to a power law component that dominates at high energies. Note also that a low-temperature disk and a significant power law component are detected in ULXs in NGC 1313 (Miller et al. 2003), for which Makishima et al. (2000) derived high  $kT$  based on a single MCD model fit to *ASCA* spectra.

The two objects NGC 5194 #69 = CXOM51 J133001.0+471344 (in 2000;  $kT=2.3$  keV,  $\log L_{\text{bol}} = 39.49$  ergs  $s^{-1}$ ) and NGC 5194 #41 = CXOM51 J132953.7+471436 (in 2001;  $kT = 2.2$  keV,  $\log L_{\text{bol}} = 39.11$  ergs  $s^{-1}$ ), and, marginally, one more object NGC 5195 #12 = CXOM51 J133006.0+471542 (in 2001;  $kT = 1.8$  keV,  $\log L_{\text{bol}} = 39.01$  ergs  $s^{-1}$ ), are not compatible with  $\eta < 1$ . They have too high a temperature compared to that expected in the MCD model from the black hole mass implied by assuming  $\eta \leq 1$ . This is the same as the “too-hot-accretion-disk problem” in ULXs (Makishima et al. 2000). This problem may be resolved if the accretion is mildly super Eddington, when a “slim disk” is expected (e.g., Watarai et al. 2000), or the black hole is rotating and we view the system near edge-on (Makishima et al. 2000; Ebisawa et al. 2001b; Mizuno et al. 2001; Ebisawa et al. 2003).

The observed luminosities and temperatures of a large fraction of the ultraluminous / luminous X-ray sources ( $L_{\text{bol}} \gtrsim 3 \times 10^{38}$  ergs  $s^{-1}$ ) imply relatively large mass accretion rates ( $0.3 < \eta < 6$ ), for which an optically-thick, thin accretion disk may not be an appropriate description. As noted above, under high accretion rates, the accretion disk may be in a slim disk branch. Fig 13 shows a comparison between MCD parameters inferred from our observations and predictions of a slim disk model in the  $L_{\text{bol}}-R_{\text{in}}$  (Fig 13a) and  $kT_{\text{in}}-R_{\text{in}}$  (Fig 13b) planes (Watarai et al. 2001, errors in the original calculations have been corrected in Fig 13). In the model,  $kT_{\text{in}}$  and  $R_{\text{in}}$  are determined by fitting a MCD model to calculated slim disk spectra. The parameters in these diagrams are the mass accretion rate  $\dot{m} = M/(L_{\text{Edd}}/c^2)$  and the black hole mass  $m = M/M_{\odot}$ . Most of the observed data points fall to the lower-mass side of the constant mass line  $m=10$  in these figures and are in good agreement

with the slim disk prediction for a mass of  $5-10M_{\odot}$  and an accretion rate  $\dot{m}=3-100$ . An interesting feature is that the data points distribute roughly along a constant mass line. This may indicate that the observed variety of values of  $L_{\text{bol}}$  and  $kT_{\text{in}}$  is mainly a result of differences in the mass accretion rate and that the black hole masses are in a relatively small range ( $5-10M_{\odot}$ ). Note, however, that the calculations by Watarai et al. do not include general relativistic effects and Compton scattering inside the disk, and that more sophisticated models would be necessary for quantitative arguments.

Although a study of spectral variability provides a good test of a slim disk scenario (Mizuno et al. 2001, Watarai et al. 2001), the errors in the obtained parameters,  $L_{\text{bol}}$ ,  $R_{\text{in}}$ , and  $kT_{\text{in}}$ , are too large to distinguish a slim disk from a thin disk model.

Mild beaming, resulting from a collimation by the inner part of the accretion disk, has been proposed as an interpretation of the apparently super Eddington luminosities of ULXs (King et al. 2001). If this is the case, objects with high  $kT_{\text{in}}$  and  $L_{\text{bol}}$  become consistent with  $\eta < 1$ , though it is not clear whether such a disk geometry is achieved for these parameters. King et al. (2001) envisage anisotropic X-ray emission from either thermal emission from a radiation pressure supported torus (e.g., Jaroszynski, Abramowicz & Paczynski 1980) or emission from a jet, however produced. Thick disks are subject to instabilities and the very existence of radiation tori is questionable. These and other issues prevent a conclusion on the relevance of beaming to ULXs.

The objects with a lower luminosity ( $L_X < 5 \times 10^{38}$  ergs  $s^{-1}$ ) and  $kT_{\text{in}} \sim 1$  keV are consistent with a thin disk picture with a stellar-mass black hole ( $\lesssim 10M_{\odot}$ ) radiating at a sub-Eddington rate (several tens of percent of the Eddington luminosity — see Fig. 12). The three objects with a slightly lower temperature,  $kT_{\text{in}} \sim 0.5$  keV (Fig. 12), have nominally higher mass ( $20-30M_{\odot}$ ) black holes and  $\eta \lesssim 10\%$ , although the errors in  $kT_{\text{in}}$ , and consequently in  $M$  and  $\eta$ , are relatively large.

Spectral information for less luminous objects was obtained from analysis of the band ratio  $C(2-8 \text{ keV})/C(0.5-2 \text{ keV})$ . Figs 5a and 5b indicate that most objects have a band ratio indicative of  $1 < \Gamma < 2$ , which is consistent with the spectra of Galactic low-mass and high-mass X-ray binary systems. A photon index of  $\Gamma \sim 1$  is slightly harder than typically observed in Galactic black hole candidates in their low/hard state. Sources with such hard spectra (Fig. 5) may have larger absorbing columns than the Galactic column or have intrinsically flat spectra.

#### 4.2.6. Unified Picture of the Luminous X-ray Sources in M51

The above discussed information about spectra and variability of individual sources does not provide strong constraints on the mass and mass accretion rates of the compact objects. In this section, we discuss possible unified pictures of the luminous X-ray sources in M51 by examining their overall ensemble properties.

A recent systematic study with *Chandra* and *XMM-Newton* of about 50 luminous X-ray sources ( $\gtrsim 5 \times 10^{38}$  ergs  $s^{-1}$ ) in various galaxies has shown that spectra of 28% and 42% of the sample are fitted better by a MCD and a power law model, respectively. The rest are well described by either a MCD or power law (Sugihara 2003). Since most of our spectra have less good photon statistics than this sample, most of the objects in M51 which are well fitted with either a MCD or power law model would thus be classified into a MCD- or a power law-type, if better signal to noise spectra were obtained. Therefore,

it is plausible that the current sample contains both classes (i.e., MCD and power law spectra).

We now discuss three possible scenarios for the luminous sources. Physically, power-law spectra may result from non-thermal processes, possibly with relativistic beaming, or through Comptonization of photons from the accretion disk.

(a) According to the MCD interpretation (discussed in section 4.2.5), the spectral parameters of most sources are compatible with stellar mass black holes ( $\lesssim 10M_{\odot}$ ) with bolometric luminosities near or above the Eddington luminosity. This interpretation is viable for at least some of the luminous sources in the present study based on the statistical results above. The state with a MCD spectrum can be identified with the high/soft state of a black hole with a thin accretion disk (Fig. 12) or a slim disk (Fig. 13), both of which show a MCD-like spectral shape, as inferred from observations of Galactic black hole candidates. The objects with a power law spectrum might be in a state with high accretion rates and significant Comptonization of photons from the accretion disk. This state might be a very high state which appears at a mass accretion rate between the values for the high/soft state of thin accretion disks and the slim disk. If this is the case, the three states can be described by a sequence of increasing mass accretion rates: the high/soft state, an apparently power-law state via strong Comptonization, and the slim disk.

(b) On the other hand, the observed power law spectra may come from black holes in a low/hard state resulting from Comptonization of disk photons in a corona or from an advection-dominated accretion flow. In this case, the mass accretion rate should be very low (less than a few % of  $L_{\text{Edd}}$ ), and then the black hole mass would be very high. For example, if a source with  $L_{\text{bol}} = 5 \times 10^{38}$  ergs  $s^{-1}$  is radiating at  $< 3\%$  of the Eddington luminosity, the black hole mass becomes  $> 100 M_{\odot}$ , in the range of IMBHs. If this is the case, a large number of IMBHs would be present in one galaxy since a significant fraction of the X-ray sources in M51 may be the power-law type, based on the spectral fits and the statistical argument of Sugihara (2003).

(c) If relativistic beaming is significant in the power-law sources, our line of sight must be within the solid angle of the beam  $\Delta\Omega$  ( $\ll 4\pi$ ). Then there must be a large number of the same class which are misaligned with respect to the line of sight. If the relativistic flow is bipolar, the number of such a class is  $2\pi N_{\text{beamed}}/\Delta\Omega \gg N_{\text{beamed}}$ , where  $N_{\text{beamed}}$  is the number of sources with the beam aligned with the line of sight. The misaligned examples might be observed as low luminosity objects with a MCD spectrum.

Although the present data cannot exclude any of these possibilities, the first one (a), in which a power law spectrum is a result of Comptonization at a high accretion rate, has the advantage that most of the objects can be explained by a sequence of fundamental parameters (black hole mass, mass accretion rate) in a relatively small range ( $M \approx 5-10M_{\odot}$  and  $\eta \approx 0.3-6$ ). On the other hand, the second and third possibilities need to introduce another population, namely IMBHs (b) and micro quasars (c), respectively.

#### 4.3. Super Soft ULXs

Two sources (NGC 5194 #9 = CXOM51 J132943.3+471135 and NGC 5195 #5 = CXOM51 J132958.4+471547) have very soft spectra and no photons were detected above 1 keV. MCD models require  $kT \sim 0.1$  keV (Table 6), which is unusually low for Galactic black hole candidates. A blackbody model pro-

vides similar temperatures (Table 9). Their luminosities exceed  $10^{38}$  ergs  $s^{-1}$  in the 0.5–8 keV band, although the errors on the luminosities are large because of the limited energy band used in the fits and strong coupling with the absorbing column. The luminosities of NGC 5194 #9 in the first observation and NGC 5195 #5 in the second observation exceed  $10^{39}$  ergs  $s^{-1}$  (for the best-fit MCD model), which is in the range of ULXs. Fig. 14 shows the data and best-fit blackbody model together with the same blackbody model after  $N_H$  has been set to 0, to demonstrate the effect of absorption.

The very soft spectra ( $kT \sim 0.1$  keV) are similar to those observed in super soft sources (SSSs) in our Galaxy and the Magellanic clouds (e.g., Kahabka & van den Heuvel 1997). The luminosities, however, are much higher than those of the typical SSS ( $10^{36} - 10^{38}$  ergs  $s^{-1}$ ). Such a soft source with a large luminosity ( $\sim 10^{39}$  ergs  $s^{-1}$  or higher) is known in M81 (Source N1, Swartz et al. 2002), the Antennae (CXOANT J120151.6–185231.9, Fabbiano et al. 2003), and M101 (P098, Mukai et al. 2003).

SSSs often show absorption edges in their spectra (Asai et al. 1998; Shimura 2000; Ebisawa et al. 2001a). Similar absorption features are detected in luminous SSSs in M81 (Swartz et al. 2002). Such features, however, are not seen in our spectra in view of the limited photon statistics. Higher quality spectra are needed to search for these absorption edges.

An optically thin thermal plasma model (MEKAL) was also examined and the results are also shown in Table 9. Although acceptable fits were obtained for NGC 5194 #9, the abundance is unphysically low (a few % of solar abundance or less) and the thermal plasma model is thus implausible.

Low temperature ( $kT \sim 0.1$  keV) and high luminosity ( $L_{\text{bol}} > 10^{39}$  ergs  $s^{-1}$ ) are just what would be expected for accretion disk emission around an IMBH. The MCD parameters derived from our model fits for NGC 5194 #9 (first observation), NGC 5194 #9 (second observation), and NGC 5195 #5 (second observation) correspond to  $R_{\text{in}} = 1.3 \times 10^5$ ,  $1.6 \times 10^4$ ,  $6.1 \times 10^4$  km;  $M_{\text{BH}} = 1.5 \times 10^4$ ,  $1.8 \times 10^3$ ,  $8.5 \times 10^3 M_{\odot}$ ;  $\eta = 0.035$ ,  $0.018$ ,  $0.041$ , respectively. This MCD interpretation has, however, two problems. First, the inner disk radius for NGC 5194 #9 decreases significantly from the first to the second observation. In a high/soft state of Galactic black hole candidates,  $R_{\text{in}}$  derived by adopting the MCD model remains constant (e.g., Ebisawa et al. 1993). The variation of  $R_{\text{in}}$  in NGC 5194 #9 suggests that a MCD interpretation is not appropriate for this object and that the parameters derived above may be unreliable. Similarly, a MCD model results in an implausibly large change in the emitting region for luminous SSSs in the Antennae (Fabbiano et al. 2003) and M101 (Mukai et al. 2003), arguing against an accretion disk around an IMBH. Second, these three spectra show no hard component. In the high/soft state of Galactic black hole candidates, a hard power-law component is always present. This component is significant at energies above 6–7 keV for a BH with  $kT_{\text{in}} \sim 1$  keV, for example. Such a hard component is also seen in IMBH candidates in NGC 1313 (Miller et al. 2003).

Mukai et al. (2003) have proposed an optically thick outflow produced by a BH radiating near the Eddington limit for an ultraluminous SSS found in M101 (source P098). Since the spectral properties and luminosities of the SSSs in M51 are quite similar to P098 in M101, the same model may be applicable to the sources in M51.

#### 4.4. The Nucleus of NGC 5195

The nucleus of NGC 5195 is classified as a LINER 2 (Ho et al. 1997). An X-ray source (NGC 5195 #7 = CXOM51 J132959.5+471559) coincides with the radio core of NGC 5195 to within the positional uncertainty ( $\sim 2''$ ) for near the edge of the CCD chip. The X-ray position is  $1''.5$  away from the radio core position, which is  $\alpha = 13^{\text{h}}29^{\text{m}}59^{\text{s}}.5$ ,  $\delta = 47^{\circ}15'57''$  (J2000) at 20 cm (Ho & Ulvestad 2001). On the other hand, the position of the optical peak ( $13^{\text{h}}29^{\text{m}}58^{\text{s}}.80$ ,  $47^{\circ}16'00''.0$  [J2000] from the Updated Zwicky Catalog [Falco et al. 1999] obtained via the NASA Extra Galactic Database) is  $7''.4$  away from the X-ray source.

Ho et al. (2001) and Georgantopoulos et al. (2002) analyzed a short (1.1 ksec exposure) *Chandra* ACIS-S3 observation of NGC 5195. Ho et al. (2001) measured an upper limit of  $< 3$  counts,  $L_X < 8.4 \times 10^{37}$  ergs  $s^{-1}$  (for a distance of 8.4 Mpc), while Georgantopoulos et al. (2002) reported detection of an X-ray nucleus with a luminosity of  $2.4 \times 10^{39}$  ergs  $s^{-1}$  in the 2–10 keV band. The X-ray nucleus found by Georgantopoulos et al. (2002) coincides with the radio core and is most probably the same source as we detect. The discrepancy between Ho et al.'s and Georgantopoulos et al.'s results may be due to the different position assumed for the nucleus in their analyses.

No long-term variability is seen between our two observations in the full, soft, or hard energy band. No short-term variability was seen within either of our observations. The number of counts found by Georgantopoulos et al. (2002) (10 counts in the 0.5–7 keV band in a 1.1 ksec exposure observation in 2000 Jan.) is consistent with the count rate we obtained in our longer observations.

The X-ray spectra obtained in 2000 and 2001 can be described by either a power law or a MCD model (see Table 7), and their spectral parameters are consistent with a low-luminosity AGN (LLAGN), an X-ray binary, or a ULX. The X-ray luminosity corrected for absorption is  $\approx 8 \times 10^{38}$  ergs  $s^{-1}$  in the 0.5–8 keV band for a power law model.

The ratio  $\log L_X/L_{\text{H}\alpha} = 0.19$  is smaller than is typical of AGNs (here  $L_X$  refers to the 2–10 keV band and the  $\text{H}\alpha$  luminosity is taken from Ho, Filippenko, & Sargent 2003). This small ratio indicates that extrapolation of the X-ray flux into the UV assuming  $f_{\nu} \propto \nu^{-1}$  (e.g., Ho 1999) provides insufficient ionizing photons to account for the  $\text{H}\alpha$  luminosity. Thus if the LINER 2 nucleus is powered by an AGN, it must be heavily obscured in the 2–10 keV band (Terashima, Ho, & Ptak 2000a; Terashima et al. 2000b).

Optical LINER spectra can be modelled in terms of photoionization by very hot stars, particularly for objects with small  $[\text{O I}]\lambda 6300/\text{H}\alpha$  ratios like NGC 5195 (Filippenko & Terlevich 1992; Shields 1992). A problem with this scenario for NGC 5195 is the absence of O stars. The optical spectrum of the nucleus of NGC 5195 shows strong Balmer absorption lines, which indicate the presence of numerous A-type stars and thus a “post-starburst” nature (Filippenko & Sargent 1985; Ho, Filippenko, & Sargent 1995; Boulade et al. 1996; Kohno et al. 2002). The age of the starburst is estimated at about  $10^9$  years. Thus, the LINER-type emission line spectrum is not likely to result from photoionization by early type main sequence or Wolf-Rayet (Filippenko 1996 and references therein; Barth & Shields 2000) stars in view of their short lifetimes.

## 5. SUMMARY

Our findings are summarized as follows.

1. We have analyzed two *Chandra* observations of M51 performed in 2000 June and 2001 June. 113 X-ray sources were detected on the ACIS-S3 CCD chip. Of these, 84 and 12 sources project within the optical extents of NGC 5194 and NGC 5195, respectively.
2. The cumulative luminosity function of the X-ray sources in NGC 5194 with  $L(0.5 - 8 \text{ keV}) > 10^{38} \text{ ergs s}^{-1}$  has a power law form  $N(> L(0.5 - 8 \text{ keV})) \propto L(0.5 - 8 \text{ keV})^{-\alpha}$ , with  $\alpha = 0.91$ , which is inbetween the typical slopes in spiral galaxies and starburst galaxies. The number of ultraluminous X-ray sources (ULXs), whose luminosities are in excess of  $10^{39} \text{ ergs s}^{-1}$  in the 0.5–8 keV band, is seven and two in NGC 5194 and NGC 5195, respectively. The number of ULXs in NGC 5194 is unusually high for spiral galaxies with mild star formation activity. The most luminous object has a luminosity of  $4 \times 10^{39} \text{ ergs s}^{-1}$  in the 0.5–8 keV band.
3. The majority of the X-ray sources are located in or near the spiral arms. All seven of the ULXs in NGC 5194 are in, or close to, a spiral arm, confirming an association with star forming activity. Five out of these seven are not coincident with bright H II regions, in contrast to some ULXs observed in starburst galaxies.
4. Short term variability within each observation was detected in three sources. About one-third of the objects in NGC 5194 or NGC 5195 varied between the two observations. Four objects exhibit large amplitude (a factor of ten or more) variability, suggesting a transient nature. One source (NGC 5194 #69) exhibits a possible period of  $\approx 2.1$  hrs in the first observation, but only two periods are covered by the observation.
5. The spectral band ratio (counts in (2–8 keV) band / counts in (0.5–2 keV) band) of most sources is consistent with a power law spectrum with a photon index of 1–2.
6. Spectral modelling was performed for 38 spectra of 26 objects, each spectrum having more than 70 counts in an observation. The spectra of the two ULXs NGC 5194 # 37 and # 82 are better described by a power law model than a multicolor disk blackbody (MCD) model. In accord with observations of ULXs in other galaxies, ULXs with a power law spectrum constitute a class of ULXs in addition to a population whose spectra are better described by a MCD. The power law spectra can be interpreted in terms of (1) the low/hard state of an accreting black hole, (2) relativistically beamed jets, or (3) emission from an accretion disk significantly Comptonized in the very high state. No strong constraints on the masses of the central objects and accretion rates have been obtained from the present data.

One transient ULX (NGC 5194 # 69) showed a drastic steepening of its spectrum, reminiscent of Galactic soft

X-ray transients. The intrinsic luminosity of this source in the 2–10 keV band decreased by a factor of 3460 from the first to the second observation. Such a drastic spectral state change and possible periodicity may provide a link to the elaborate phenomenology of stellar mass black hole candidates.

One ULX (NGC 5194 # 26) displayed strong emission lines from highly ionized species in the first observation; these lines disappeared in the second observation, when the luminosity was 50% higher than in the first observation.

The spectra of the other ULXs and less luminous sources may be described by either a power law or a MCD model. If we adopt the MCD model, their spectral parameters are consistent with an accretion disk around a black hole with a mass of 5–10  $M_{\odot}$  accreting at near or above the Eddington rate.

There are three sources with very soft spectra ( $kT \approx 0.15$  keV). Their inferred X-ray luminosities ( $4.0 \times 10^{38} - 2.6 \times 10^{39} \text{ ergs s}^{-1}$ ) are unusually high compared to super soft sources known so far. We discuss the idea that this soft emission originates in an accretion disk around an intermediate mass black hole.

7. From the spectral properties of the luminous sources (except the sources with very soft spectra), we speculate that they are stellar-mass black holes radiating around or above the Eddington luminosity. In this scenario, sources with a power law spectrum can be interpreted in terms of Comptonized accretion disk emission when accretion rates are high. X-ray emission from sources best described by a MCD model originates in the optically-thick geometrically-thin accretion disk or slim disk. Alternatively, sources with power law spectra may be in a “low/hard” state, in which case the black hole mass becomes  $> 100 M_{\odot}$ , and in the range of intermediate-mass black holes. Another possibility is that the emission from the power-law sources originates in a relativistic jet.
8. The LINER 2 nucleus of NGC 5195 may be powered by a heavily obscured AGN and/or shocks. The gas radiating the narrow emission lines is unlikely to be photoionized by O stars.

The authors are grateful to D. A. Thilker for providing optical images and a list of H II regions in computer readable format. We wish to thank K. Watarai for his slim disk calculations, and A. Kubota for her useful input. M. C. Miller gave valuable comments on the manuscript. Y. T. is supported by the Japan Society for the Promotion of Science. This research was supported by NASA through grants NAG81027 and NAG81755 to the University of Maryland.

#### REFERENCES

- Angelini, L., Loewenstein, M., Mushotzky, R. F. 2001, *ApJ*, 557, L35  
 Asai, K., Dotani, T., Nagase, F., Ebisawa, K., Mukai, K., Smale, A. P., & Kotani, T. 1998, *ApJ*, 503, L143  
 Barth, A. J. & Shields, J. C. 2000, *PASP*, 112, 753  
 Bauer, F. E., Brandt, W. N., Sambruna, R. M., Chartas, G., Garmire, G. P., Kaspi, S., & Netzer, H. 2001, *AJ*, 122, 182  
 Begelman, M. C., 2002, *ApJ*, 568, 97  
 Blanton, E. L., Sarzin, C. L., & Irwin, J. A. 2001, *ApJ*, 552, 106  
 Boulade, O. et al. 1996, *A&A*, 315, L85  
 Brandt, W. N. et al. 2001, *AJ*, 122, 2810  
 Cash, W. 1979, *ApJ*, 228, 939  
 Colbert, E. J. M. & Ptak, A. F. 2002, *ApJS*, 143, 25

- Di Stefano, R., Kong, A. K. H., VanDalsen, M. L., Harris, W. E., Murray, S. S., & Delain, K. M. 2003, *ApJ*, submitted (astro-ph/0306441)
- Done, C. 2002, *Phil. Trans. Royal Soc.*, A360, 1967 (astro-ph/0203246)
- Dotani, T. et al. 1997, *ApJ*, 485, L87
- Ebisawa, K. et al. 1996, *PASJ*, 48, 425
- 2001a, *ApJ*, 550, 1007
- Ebisawa, K., Kubota, A., Mizuno, T., & Życki, P. 2001b, *Ap&SS Suppl.* 276, p.11
- Ebisawa, K., Makino, F., Mitsuda, K., Belloni, T., Cowley, A. P., Schmidtke, P. C., & Treves, A. 1993, *ApJ*, 403, 684
- Ebisawa, K., Życki, P., Kubota, A., Mizuno, T., & Watarai, K. 2003, *ApJ*, in press (astro-ph/0307392)
- Ehle, M., Pietsch, W., & Beck, R. 1995, *A&A*, 295, 289
- Fabbiano, G. 1996, *MPE report* 263, 347
- Fabbiano, G., King, A. R., Zezas, A., Ponman, T. J., Rots, A., & Schweizer, F. 2003, *ApJ*, 591, 843
- Fabbiano, G., Zezas, A., King, A. R., Ponman, T. J., Rots, A. R., Schweizer, F. 2003, *ApJ*, 584, L5
- Fabbiano, G., Zezas, A., & Murray, S. S. 2001, *ApJ*, 554, 1035
- Falco, E. et al. 1999, *PASP*, 111, 438
- Feldmeier, J. J., Ciardullo, R., & Jacoby, G. 1997, *ApJ*, 479, 231
- Filippenko, A. V. 1996, in *ASP conf. Ser. 103, The Physics of LINERs in View of Recent Observations*, ed. M. Eracleous et al. (San Francisco: ASP), 17
- Filippenko, A. V., & Sargent, W. L. W. 1985, *ApJS*, 57, 503
- Filippenko, A. V., & Terlevich, R. 1992, *ApJ*, 397, L79
- Foschini, L., et al. 2003, in *New Visions of the X-ray Universe in the XMM-Newton and Chandra Era*, ed. F. Jansen
- Fukazawa, Y., Iyamoto, N., Kubota, A., Matsumoto, Y., & Makishima, K. 2001, *A&A*, 374, 73
- Gehrels, N. 1986, *ApJ*, 303, 336
- Georgantopoulos, I., Panessa, F., Akylas, A., Zezas, A., Cappi, M., & Comastri, A. 2002, *A&A*, 386, 60
- Greenawalt, B., Walterbos, R. A. M., Thikler, D., & Hoopes, C. G. 1998, *ApJ*, 506, 135
- Griffiths, R., et al. 2000, *Science*, 290, 1325
- Ho, L. C. 1999, *ApJ*, 516, 672
- Ho, L. C., et al. 2001, *ApJ*, 549, L51
- Ho, L. C., Filippenko, A. C., & Sargent, W. L. W. 1995, *ApJS*, 98, 477
- 1997, *ApJS*, 112, 315
- 2003, *ApJ*, 583, 159
- Ho, L. C. & Ulvestad, J. S. 2001, *ApJS*, 133, 77
- Immler, S. & Lewin, W. H. G. 2002, “Supernovae and Gamma-Ray Bursts”, ed., K. W. Weiler (Springer-Verlag)
- Irwin, J. A., Sarazin, C. L., & Bregman, J. N. 2002, *ApJ*, 570, 152
- Jaroszynski, M., Abramowicz, M. A., & Paczynski, B. 1980, *Acta Astron.*, 30, 1
- Kaaret, P. et al. 2001, *MNRAS*, 321, L29
- Kahabka, P., & van den Heuvel, E. P. J. 1997, *ARA&A*, 35, 69
- Kaiser, M. E., Baam, W. A., & Bradley, L. D. II 2001, in preparation
- Kilgard, R. E., Kaaret, P., Krauss, M. I., Prestwich, A. H., Raley, M. T., & Zezas, A. 2002, *ApJ*, 573, 138
- Kim, D.-W., & Fabbiano, G. 2003, *ApJ*, 586, 826
- King, A. R., Davies, M. B., Ward, M. J., Fabbiano, G., & Elvis, M. 2001, *ApJ*, 552, L109
- King, A. R. 2002, *MNRAS*, 335, L13
- Kohno, K., Tosaki, T., Matsushita, S., Vila-Vilaró, B., Shibatsuka, T., & Kawabe, R. 2002, *PASJ*, 54, 541
- Kong, A. K. H., Garcia, M. R., Primini, F. A., Murray, S. S., Di Stefano, R., & McClintock, J. E. 2002, *ApJ*, 577, 738
- Körding, E., Falcke, H., & Markoff, S. 2002, *A&A*, 382, L13
- Kraft, R. P., Burrows, D. N., & Nousek, J. A. 1991, *ApJ*, 374, 344
- Kubota, A. 2001, Ph.D. thesis, The University of Tokyo
- Kubota, A., Done, C., & Makishima, K. 2002, *MNRAS*, 337, L11
- Kubota, A., Mizuno, T., Makishima, K., Fukazawa, Y., Kotoku, J., Ohnishi, T., & Tashiro, M. 2001a, *ApJ*, 547, L119
- Kubota, A., Makishima, K., & Ebisawa, K. 2001b, *ApJ*, 560, L147
- Kubota, A., Tanaka, Y., Makishima, K., Ueda, Y., Dotani, T., Inoue, H., & Yamaoka, K. 1998, *PASJ*, 50, 667
- Kundu, A., Maccarone, T. J., & Zepf, S. E. 2002, *ApJ*, 574, L5
- Lamers, H. J. G. L. M., Panagia, N., Scuderi, S., Romaniello, M., Spaans, M., De Wit, W. J., & Kirshner, R. 2002, *ApJ*, 566, 818
- Lira, P., Ward, M., Zezas, A., Alonso-Herrero, & Ueno, S. 2002, *MNRAS*, 330, 259
- Liu, J.-F., Bregman, J. N., Irwin, J., & Seitzer, P. 2002, *ApJ*, 581, L93
- Makishima, K. et al. 1986, *ApJ*, 308, 635
- 2000, *ApJ*, 535, 632
- Matsumoto, H. et al. 2001, *ApJ*, 547, L25
- Marston, A. P., Elmegreen, D., Elmegreen, B., Forman, W., Jones, C., & Flanagan, K. 1995, *ApJ*, 438, 663
- Miller, J. M., Fabbiano, G., Miller, M. C., & Fabian, A. C. 2003, *ApJ*, 585, L37
- Mitsuda, K. et al. 1984, *PASJ*, 36, 741
- Miyaji, T., Lehmann, I., & Hasinger, G. 2001, *AJ*, 121, 3041
- Mizuno, T., Kubota, A., & Makishima, K. 2001, *ApJ*, 554, 1282
- Mukai, K., Pence, W. D., Snowden, S. L., & Kuntz, K. D. 2003, *ApJ*, 582, 184
- Mushotzky, R. F., Cowie, L. L., Barger, A. J., & Arnaud, K. A. 2000, *Nature*, 404, 459
- Nagase, F., Zylstra, G., Sonobe, T., Kotani, T., Inoue, H., & Woo, J. 1994, *ApJ*, 436, L1
- Palumbo, G. C. C., Fabbiano, G., Fransson, C., & Trinchieri, G. 1985, *ApJ*, 298, 259
- Read, A. M., Ponman, T. J., & Strickland, D. K. 1997, *MNRAS*, 1997, 286, 626
- Reynolds, C. S., Loan, A. J., Fabian, A. C., Makishima, K., Brandt, W. N. & Mizuno, T. 1997, *ApJ*, 286, 349
- Roberts, T. P. & Warwick, R. S. 2000, *MNRAS*, 315, 98
- Roberts, T. P., Goad, M. R., Ward, M. J., Warwick, R. S., O’Brien, P. T., Lira, P., & Hands, A. D. P. 2001, *MNRAS*, 325, L7
- Sako, M., Liedahl, D. A., Kahn, S. M., & Paerels, F. 1999, *ApJ*, 525, 921
- Sarazin, C. L., Irwin, J. A., & Bregman, J. N. 2000, *ApJ*, 544, L101
- Schulz, N. S., Canizares, C. R., Lee, J. C., & Sako, M. 2002, *ApJ*, 564, L21
- Scoville, N. Z., Polletta, M., Ewald, S., Stolovy, S. R., Thompson, R., & Rieke, M. 2001, *AJ*, 122, 3017
- Shields, J. C. 1992, *ApJ*, 399, L27
- Shimura, T. 2000, *MNRAS*, 315, 345
- Shimura, T. & Takahara, F. 1995, *ApJ*, 445, 780
- Smith, D. A., & Wilson, A. S. 2001, *ApJ*, 557, 180
- 2003, *ApJ*, 591, 138
- Stark, A. A., Gammie, C. F., Wilson, R. W., Bally, J., Linke, R. A., Heiles, C., & Hurwitz, M. 1992, *ApJS*, 79, 77
- Strickland, D. K., Colbert, E. J. M., Heckman, T. M., Weaver, K. A., Dahlem, M., & Stevens, I. R. 2001, *ApJ*, 560, 707
- Sugihō, M. 2003, Ph.D. thesis, The University of Tokyo
- Swartz, D. A., Ghosh, K. K., McCollough, M. L., Pannuti, T. G., Tennant, A. F., & Wu, K. 2003, *ApJS*, 144, 213
- Swartz, D. A., Ghosh, K. K., Suleimanov, V., Tennant, A. F., & Wu, K. 2002, *ApJ*, 574, 382
- Tanaka, Y. 1996, “Accretion Disks - New Aspects”, eds. E. Meyer-Hofmeister and H. Spruit, 1 (Springer)
- Tanaka, Y. & Shibazaki, N. 1996, *ARA&A*, 34, 607
- Tennant, A. F., Wu, K., Ghosh, K. K., Kolodziejczak, J. J., & Swartz, D. A. 2001, *ApJ*, 549, L43
- Terashima, Y., Ho, L. C., & Ptak, A. F. 2000a, *ApJ*, 539, 161
- Terashima, Y., Ho, L. C., Ptak, A. F., Mushotzky, R. F., Serlemitsos, P. J., Yaqoob, T., & Kunieda, H. 2000b, *ApJ*, 533, 729
- Terashima, Y., & Wilson, A. S. 2001, *ApJ*, 560, 139
- Thilker, D. A., Robert, B., & Walterbos, R. A. M. 2000, *AJ*, 120, 3070
- Tozzi, P., et al. 2001, *ApJ*, 562, 42
- Watarai, K., Mizuno, T., & Mineshige, S. 2001, *ApJ*, 549, L77
- Watarai, K., Fukue, J., Takeuchi, M., & Mineshige, S. 2000, *PASJ*, 52, 133
- Wu, K., Tennant, A. F., Swartz, D. A., Ghosh, K. K., & Hunstead, R. W. 2003, in *New Visions of the X-ray Universe in the XMM-Newton and Chandra Era*, ed. F. Jansen
- Zezas, A., & Fabbiano, G. 2002, *ApJ*, 577, 726

TABLE 1  
NUMBER OF DETECTED SOURCES

Location	Energy Band							
	(0.5–8 keV)		(0.5–2 keV)		(2–8 keV)		(Any One of the Three Bands)	
	Detected	Variable	Detected	Variable	Detected	Variable	Detected	Variable
S3 chip	113	32	102	30	48	15	113	36
NGC 5194	84	26	76	22	34	14	84	28
NGC 5195	12	3	11	3	8	0	12	3

TABLE 2  
SOURCES SPATIALLY COINCIDENT WITH NGC 5194

No. (1)	RA (J2000) (2)	Dec. (J2000) (3)	CXO Name CXOM51 (4)	Counts (Observations 1+2)			Counts (Observation 1)			Counts (Observation 2)		
				0.5–8 keV (5)	0.5–2 keV (6)	2–8 keV (7)	0.5–8 keV (8)	0.5–2 keV (9)	2–8 keV (10)	0.5–8 keV (11)	0.5–2 keV (12)	2–8 keV (13)
1	13 29 35.69	47 12 01.1	J132935.7+471201	15.2±5.4	<9.4	11.6±4.7	<14.0	<4.3	6.6±3.8	8.2±4.3	<8.7	<11.2
2	13 29 36.55	47 11 05.4	J132936.5+471105	8.8±4.6	6.7±2.6	<7.9	<6.6	<5.7	<4.4	<14.3	<11.1	<7.0
3	13 29 38.92	47 13 23.9	J132938.9+471324	54.6±8.8	37.5±7.3	17.4±4.2	16.6±4.1	12.9±3.6	<8.9	38.5±7.6	24.9±6.2	13.6±3.7
4	13 29 38.98	47 11 03.6	J132939.0+471104	26.3±5.2	16.6±4.1	9.7±3.2	14.7±5.0	8.9±3.0	<12.2	12.7±3.6	7.9±2.8	<10.4
5	13 29 39.45	47 12 43.7	J132939.5+471244	427±21	308±18	120±11	244±16	170±13	73.6±8.6	184±14	138±12	46.5±6.9
6	13 29 39.96	47 12 36.9	J132940.0+471237	276±17	266±16	10.4±4.4	226±15	217±15	8.8±4.1	50.0±7.1	48.3±7.0	<5.9
7	13 29 41.65	47 10 52.3	J132941.6+471052	20.4±4.6	16.6±4.1	<8.9	<9.0	<6.1	<6.2	16.6±4.1	14.7±3.9	<5.9
8	13 29 42.51	47 10 42.7	J132942.5+471043	16.7±5.3	13.1±4.8	<9.1	<10.3	<9.0	<4.6	12.3±4.7	9.5±4.3	<7.7
9	13 29 43.30	47 11 34.7	J132943.3+471135	365±19	364±19	<5.8	147±12	146±12	<4.6	219±15	218±15	<4.5
10	13 29 44.05	47 11 56.4	J132944.1+471156	18.8±5.7	17.3±5.4	<5.8	8.2±4.1	7.3±4.0	<4.6	10.6±4.6	9.9±4.4	<4.5
11	13 29 44.19	47 10 20.3	J132944.2+471020	8.1±4.4	8.7±4.4	<4.3	<8.3	<8.6	<4.6	<11.7	<12.0	<4.5
12	13 29 44.55	47 13 56.7	J132944.5+471357	72.8±8.6	55.4±8.6	18.6±4.4	14.8±3.9	10.5±4.4	<10.0	58.1±7.7	43.9±7.8	13.7±3.7
13	13 29 44.87	47 11 28.6	J132944.9+471129	11.8±4.8	7.3±4.1	<10.3	<10.0	<8.8	<4.6	<14.9	<9.8	<9.1
14	13 29 45.51	47 11 51.0	J132945.5+471151	30.0±5.6	14.3±3.9	15.7±4.0	12.7±3.6	6.8±2.6	5.9±2.4	17.3±4.2	7.6±2.8	9.8±3.2
15	13 29 45.52	47 11 25.2	J132945.5+471125	11.3±3.5	8.5±3.0	<7.4	<4.2	<4.3	<4.6	10.5±3.3	8.7±3.0	<6.0
16	13 29 45.94	47 10 55.7	J132945.9+471056	9.0±3.2	7.5±2.8	<5.8	<7.0	<7.2	<4.6	<13.6	<11.2	<6.0
17	13 29 46.11	47 10 42.3	J132946.1+471042	28.6±5.5	25.0±5.1	<8.9	26.6±5.2	23.7±4.9	<7.8	<6.4	<5.4	<4.5
18	13 29 47.02	47 11 04.3	J132947.0+471104	11.8±4.8	12.3±4.8	<4.4	<8.6	<8.8	<4.6	8.6±4.3	8.9±4.3	<4.5
19	13 29 47.51	47 13 01.3	J132947.5+471301	17.8±4.4	10.5±3.3	7.5±4.0	16.2±5.2	9.3±4.3	6.9±2.6	<5.1	<4.1	<4.5
20	13 29 48.79	47 11 21.4	J132948.8+471121	67.8±9.4	50.3±8.3	17.7±4.2	18.2±5.4	15.3±5.1	<7.8	49.6±8.2	34.9±7.1	14.8±3.9
21	13 29 49.03	47 10 53.3	J132949.0+471053	143±12	105±10	36.5±6.1	<5.6	<5.7	<4.6	142±12	104±10	36.7±6.1
22	13 29 49.15	47 12 57.0	J132949.2+471257	14.0±3.9	<3.9	13.7±3.7	8.7±3.0	<4.3	8.9±3.0	<10.8	<4.1	<10.5
23	13 29 50.06	47 14 19.9	J132950.1+471420	17.7±5.7	16.0±5.3	<6.5	<12.5	<12.9	<4.4	<19.4	8.8±3.0	<7.0
24	13 29 50.08	47 11 39.3	J132950.1+471139	32.3±6.2	31.8±6.1	<4.2	12.0±3.9	12.5±3.9	<4.5	21.8±5.0	20.7±4.9	<4.3
25	13 29 50.35	47 13 22.7	J132950.4+471323	22.8±6.1	22.3±6.0	<4.4	<12.8	<11.6	<4.6	16.6±5.3	16.9±5.3	<4.5
26	13 29 50.67	47 11 55.1	J132950.7+471155	377±20	52.2±9.0	325±18	104±11	<19.2	95.6±9.8	273±17	42.8±8.1	229±15
27	13 29 50.82	47 10 31.3	J132950.8+471031	135±13	117±11	17.5±5.3	71.2±9.5	61.4±7.9	9.8±4.3	63.6±9.1	55.9±8.6	7.7±4.0
28	13 29 51.36	47 10 32.4	J132951.4+471032	238±16	155±13	83±10	73.2±9.6	48.4±8.1	24.8±6.1	165±13	107±10	58.6±7.7
29	13 29 51.78	47 11 52.0	J132951.8+471152	36.3±8.1	36.2±8.0	<4.2	13.1±5.3	13.4±5.3	<4.5	24.2±6.7	23.8±6.6	<4.3
30	13 29 52.07	47 11 26.8	J132952.1+471127	24.3±7.1	25.2±7.1	<4.2	<16.7	<17.6	<4.5	18.8±4.9	19.1±4.9	<4.3
31	13 29 52.12	47 12 12.8	J132952.1+471213	22.1±5.3	21.7±5.2	<5.7	8.2±4.6	<15.2	<4.7	12.6±3.9	12.8±3.9	<4.4
32	13 29 52.23	47 11 29.6	J132952.2+471130	25.3±7.2	24.2±7.1	<5.5	<16.7	<17.6	<4.5	17.2±6.1	15.8±5.9	<5.8
33	13 29 52.73	47 10 51.2	J132952.7+471051	34.0±6.0	15.8±4.1	18.5±5.4	14.2±5.0	<10.2	9.9±3.2	19.9±4.6	10.9±4.6	8.7±3.0
34	13 29 52.73	47 11 21.4	J132952.7+471121	16.1±4.6	15.0±4.5	<4.2	<6.4	<5.6	<4.5	12.7±4.0	12.8±4.0	<4.3
35	13 29 52.75	47 10 42.6	J132952.7+471043	11.8±4.8	<15.9	<8.9	8.2±4.1	<13.0	<6.2	<9.3	<6.7	<6.0
36	13 29 52.79	47 12 44.9	J132952.8+471245	42.8±7.8	28.3±6.5	14.5±5.0	30.2±6.6	20.4±5.7	9.9±3.2	12.6±4.8	<15.2	<10.5
37	13 29 53.31	47 10 42.3	J132953.3+471042	581±24	429±21	151±12	<5.6	<5.7	<4.6	581±24	429±21	151±12
38	13 29 53.53	47 11 32.9	J132953.5+471133	27.3±7.4	19.2±6.6	8.1±4.1	<21.0	<14.4	<10.5	15.5±4.6	11.9±4.1	<8.9

TABLE 2—Continued

No. (1)	RA (J2000) (2)	Dec. (J2000) (3)	CXO Name CXOM51 (4)	Counts (Observations 1+2)			Counts (Observation 1)			Counts (Observation 2)		
				0.5–8 keV (5)	0.5–2 keV (6)	2–8 keV (7)	0.5–8 keV (8)	0.5–2 keV (9)	2–8 keV (10)	0.5–8 keV (11)	0.5–2 keV (12)	2–8 keV (13)
39	13 29 53.54	47 11 26.4	J132953.5+471126	36.2±6.6	32.1±6.2	<11.4	12.6±3.9	11.8±3.7	<6.0	22.7±5.2	19.8±4.8	<8.9
40	13 29 53.62	47 13 22.8	J132953.6+471323	12.0±3.6	12.3±3.6	<4.4	<14.2	<14.3	<4.6	<10.8	<11.2	<4.5
41	13 29 53.72	47 14 35.9	J132953.7+471436	629±26	445±22	184±15	227±16	165±14	62.1±9.0	401±21	279±18	122±12
42	13 29 53.79	47 14 31.7	J132953.8+471432	276±18	217±16	58.9±8.9	114±12	92±11	<33.8	164±14	127±12	36.8±7.2
43	13 29 53.93	47 10 31.3	J132953.9+471031	12.7±3.7	13.3±5.0	<4.4	<4.2	<4.3	<4.6	12.6±4.8	12.9±4.8	<4.5
44	13 29 54.00	47 09 23.3	J132954.0+470923	9.6±4.4	8.2±4.1	<5.8	<7.4	<6.1	<4.6	<14.1	<13.1	<4.5
45	13 29 54.16	47 11 30.2	J132954.2+471130	18.3±6.6	16.2±6.4	<6.9	<16.7	<14.4	<6.0	11.2±5.4	9.8±5.2	<5.8
46	13 29 54.18	47 11 37.0	J132954.2+471137	111±12	68.0±8.9	43.1±7.7	44.1±6.9	26.7±5.5	17.7±4.2	68.2±9.8	42.8±8.1	25.5±6.2
47	13 29 54.24	47 13 00.2	J132954.2+471300	47.2±7.0	15.0±4.0	32.5±6.8	18.5±4.4	7.7±2.8	10.9±3.3	29.0±5.5	7.4±2.8	21.7±4.7
48	13 29 54.37	47 11 21.5	J132954.4+471122	26.8±5.7	27.5±5.7	<4.2	11.8±3.6	11.9±3.6	<4.5	13.9±4.1	14.2±4.1	<4.3
49	13 29 54.53	47 09 21.6	J132954.5+470922	69.2±8.4	45.7±6.9	23.6±4.9	25.5±5.1	17.7±4.2	7.9±2.8	42.0±6.6	26.4±5.2	15.8±4.0
50	13 29 54.96	47 09 22.4	J132955.0+470922	47.6±7.0	38.1±6.2	9.5±4.3	16.5±5.2	12.7±3.6	<9.2	31.2±5.7	25.4±6.2	5.9±2.4
51	13 29 54.99	47 11 02.2	J132955.0+471102	12.5±3.7	10.8±3.5	<5.8	7.7±2.8	<11.6	<6.2	<10.8	<11.2	<4.5
52	13 29 55.13	47 10 42.2	J132955.1+471042	29.8±6.7	29.3±6.6	<4.4	8.6±3.0	7.3±4.0	<4.6	21.6±5.9	21.9±5.9	<4.5
53	13 29 55.24	47 10 46.2	J132955.2+471046	8.1±3.0	8.3±3.0	<4.4	<7.0	<7.2	<4.6	<10.8	<11.2	<4.5
54	13 29 55.45	47 11 43.5	J132955.5+471143	49.6±7.5	45.4±7.2	<10.0	11.3±3.6	11.5±3.6	<4.5	37.2±7.8	32.8±7.4	<10.3
55	13 29 55.47	47 14 02.0	J132955.5+471402	16.6±4.2	16.2±5.5	<4.1	10.5±4.6	9.8±4.4	<4.5	<12.8	<13.5	<4.3
56	13 29 55.63	47 09 18.7	J132955.6+470919	7.6±4.1	<11.4	<7.4	<5.8	<4.5	<4.6	<12.8	<10.3	<6.0
57	13 29 55.66	47 09 10.6	J132955.7+470911	12.8±5.2	12.4±5.0	<5.0	<4.0	<4.2	<4.3	13.3±5.1	12.3±4.8	<5.4
58	13 29 55.70	47 10 43.6	J132955.7+471044	14.8±5.2	14.3±5.1	<4.4	<12.8	<13.0	<4.6	9.1±3.2	8.4±3.0	<4.5
59	13 29 55.86	47 11 44.5	J132955.9+471145	42.5±6.9	41.5±6.9	<4.2	13.8±3.9	13.0±3.7	<4.5	27.0±5.6	27.4±5.6	<4.3
60	13 29 56.06	47 13 50.9	J132956.1+471351	14.8±4.0	15.1±4.0	<4.2	<12.5	<11.3	<4.6	8.5±4.3	9.0±4.3	<4.4
61	13 29 56.15	47 12 36.6	J132956.1+471237	18.8±5.7	18.3±5.6	<4.4	<10.0	<8.8	<4.6	14.6±5.1	14.9±5.1	<4.5
62	13 29 57.47	47 10 37.1	J132957.5+471037	18.8±5.7	18.9±4.5	<4.4	<12.8	<13.0	<4.6	13.2±3.7	12.4±3.6	<4.5
63	13 29 57.57	47 10 48.3	J132957.6+471048	400±20	318±18	81±10	118±11	92±11	25.8±6.2	282±17	226±15	55.6±7.5
64	13 29 57.62	47 12 06.2	J132957.6+471206	95±11	73.9±8.7	20.6±4.6	92.1±9.6	72.3±8.5	19.8±5.6	<7.8	<6.7	<4.5
65	13 29 58.36	47 13 20.5	J132958.4+471321	76.1±8.8	53.6±7.4	22.6±4.8	32.4±5.7	20.6±4.6	11.9±3.5	43.8±6.7	33.1±6.9	10.7±4.4
66	13 29 58.72	47 10 29.9	J132958.7+471030	53.8±7.4	27.2±5.3	26.5±5.2	32.6±5.7	16.4±5.2	15.9±4.0	21.2±4.7	10.6±3.3	10.7±4.4
67	13 29 59.02	47 14 34.2	J132959.0+471434	12.5±5.2	<15.0	<11.7	11.4±4.7	<14.0	<10.2	<6.5	<5.0	<5.2
68	13 30 00.56	47 11 36.0	J133000.6+471136	13.2±5.1	<20.7	<5.7	<12.5	<11.4	<4.6	<14.6	<13.7	<4.5
69	13 30 01.02	47 13 44.0	J133001.0+471344	553±24	374±20	180±13	507±23	336±18	171±13	46.3±7.0	38.0±6.3	<13.3
70	13 30 01.12	47 13 32.9	J133001.1+471333	12.4±5.1	12.2±3.7	<4.4	<7.8	<8.0	<4.6	9.8±4.6	9.1±3.2	<4.5
71	13 30 01.27	47 12 44.2	J133001.3+471244	15.2±4.1	<14.1	<11.8	<7.0	<5.7	<4.6	10.2±3.3	<12.1	<10.6
72	13 30 01.88	47 08 43.7	J133001.9+470844	10.4±4.7	11.6±4.7	<4.0	<9.9	<10.4	<4.3	<13.3	<14.0	<4.3
73	13 30 02.10	47 12 38.1	J133002.1+471238	17.6±4.4	15.0±4.0	<7.4	10.1±4.4	10.3±4.4	<4.6	<13.2	<9.2	<7.6
74	13 30 02.13	47 09 00.6	J133002.1+470901	40.9±6.5	29.6±6.6	10.6±4.6	<5.5	<5.9	<4.4	40.2±6.4	28.1±6.5	11.0±4.6
75	13 30 04.10	47 10 03.5	J133004.1+471003	24.2±6.5	24.7±6.4	<3.9	13.4±5.0	12.9±4.9	<4.4	10.8±4.9	11.9±4.9	<4.1
76	13 30 04.32	47 13 20.8	J133004.3+471321	120±11	78.2±9.0	41.5±7.6	<9.1	<8.2	<4.4	115±11	74.3±8.7	40.9±7.5

TABLE 2—*Continued*

No. (1)	RA (J2000) (2)	Dec. (J2000) (3)	CXO Name CXOM51 (4)	Counts (Observations 1+2)			Counts (Observation 1)			Counts (Observation 2)		
				0.5–8 keV (5)	0.5–2 keV (6)	2–8 keV (7)	0.5–8 keV (8)	0.5–2 keV (9)	2–8 keV (10)	0.5–8 keV (11)	0.5–2 keV (12)	2–8 keV (13)
77	13 30 04.47	47 10 31.4	J133004.5+471031	31.9±5.7	30.3±5.6	<5.9	14.8±5.0	12.8±4.7	<6.3	17.4±4.2	17.6±4.2	<4.5
78	13 30 04.66	47 14 17.0	J133004.7+471417	64.1±9.4	48.0±7.1	15.9±5.2	31.6±6.8	23.8±6.1	<14.8	33.6±5.9	25.9±5.2	8.2±4.1
79	13 30 05.82	47 10 31.9	J133005.8+471032	13.1±3.7	13.4±3.7	<4.1	<15.6	<16.0	<4.4	<7.5	<8.1	<4.2
80	13 30 06.04	47 14 04.0	J133006.0+471404	24.3±6.5	23.7±6.3	<5.2	<17.2	<16.4	<4.3	15.0±5.4	14.8±5.2	<4.2
81	13 30 06.27	47 10 16.4	J133006.3+471016	9.6±4.9	<11.7	<10.9	<9.1	<5.3	<7.5	<13.4	<10.2	<6.9
82	13 30 07.56	47 11 05.9	J133007.6+471106	1680±42	1367±38	312±18	831±30	688±26	139±13	845±29	673±26	174±14
83	13 30 08.89	47 12 18.5	J133008.9+471218	29.0±5.6	24.8±5.1	<9.9	<9.2	<8.2	<4.4	24.0±5.0	20.3±4.6	<9.0
84	13 30 11.03	47 10 40.7	J133011.0+471041	89.3±9.5	65.1±9.2	24.6±6.2	32.1±6.8	23.6±6.0	8.5±4.1	57.6±8.7	41.6±6.5	16.1±5.2

TABLE 3  
SOURCES SPATIALLY COINCIDENT WITH NGC 5195

No. (1)	RA (J2000) (2)	Dec. (J2000) (3)	CXO Name CXOM51 (4)	Counts (Observations 1+2)			Counts (Observation 1)			Counts (Observation 2)		
				0.5–8 keV (5)	0.5–2 keV (6)	2–8 keV (7)	0.5–8 keV (8)	0.5–2 keV (9)	2–8 keV (10)	0.5–8 keV (11)	0.5–2 keV (12)	2–8 keV (13)
1	13 29 52.80	47 16 44.5	J132952.8+471644	157±13	103±11	54.7±8.7	55.7±8.7	38.9±7.4	16.8±5.4	102±11	64.0±9.2	37.8±7.4
2	13 29 55.53	47 15 55.4	J132955.5+471555	22.2±5.3	<8.4	20.8±6.0	<12.2	<6.2	<9.8	17.0±6.1	<6.4	16.9±5.5
3	13 29 57.06	47 15 56.5	J132957.1+471556	25.5±8.8	19.6±7.9	<13.4	<18.8	<15.4	<8.7	14.0±7.3	12.4±6.7	<7.3
4	13 29 57.48	47 16 12.1	J132957.5+471612	256±17	178±16	74.1±9.9	100±12	69±10	30.5±6.7	153±13	109±13	43.5±7.8
5	13 29 58.38	47 15 47.4	J132958.4+471547	124±14	120±14	<9.3	50.6±9.2	49.0±9.1	<6.4	75±11	74±11	<6.9
6	13 29 58.74	47 16 25.5	J132958.7+471625	94±13	88±12	<13.6	<12.0	<12.0	<4.0	92±12	85±11	<15.1
7	13 29 59.53	47 15 58.5	J132959.5+471559	522±25	390±22	132±13	176±15	130±13	45.5±7.9	345±20	258±18	88±11
8	13 29 59.79	47 15 40.8	J132959.8+471541	89±13	66±11	22.1±6.2	29.6±7.9	25.0±7.4	<10.8	59±10	41.5±9.2	<28.3
9	13 30 00.62	47 15 30.5	J133000.6+471530	19.5±5.2	18.8±5.0	<6.7	22.5±5.3	20.3±4.9	<6.7	<8.0	<7.0	<4.1
10	13 30 02.02	47 15 06.3	J133002.0+471506	96±11	68.0±9.4	28.1±6.6	34.6±7.1	26.3±6.3	8.2±4.1	61.5±9.1	41.7±7.6	19.7±5.7
11	13 30 03.76	47 16 11.2	J133003.8+471611	85±11	75±10	9.9±4.8	<7.9	<6.2	<5.4	83±11	74.1±9.9	8.9±4.5
12	13 30 06.03	47 15 42.4	J133006.0+471542	547±25	386±21	161±14	200±15	150±13	50.8±8.3	347±20	237±17	110±12

TABLE 4  
OTHER SOURCES

No. (1)	RA (J2000) (2)	Dec. (J2000) (3)	CXO Name CXOM51 (4)	Counts (Observations 1+2)			Counts (Observation 1)			Counts (Observation 2)		
				0.5–8 keV (5)	0.5–2 keV (6)	2–8 keV (7)	0.5–8 keV (8)	0.5–2 keV (9)	2–8 keV (10)	0.5–8 keV (11)	0.5–2 keV (12)	2–8 keV (13)
1	13 29 26.63	47 12 34.5	J132926.6+471235	9.7±4.8	<14.9	<7.3	<10.8	<10.4	<4.1	<11.7	<8.3	<6.9
2	13 29 33.33	47 14 40.4	J132933.3+471440	18.7±5.8	10.3±4.4	<16.3	<15.7	<12.2	<7.5	10.2±4.8	4.4±3.4	<12.7
3	13 29 36.77	47 14 48.5	J132936.8+471448	22.0±6.3	20.7±5.9	<6.7	12.8±5.0	<19.2	<6.6	8.3±4.5	9.7±4.5	<4.0
4	13 29 37.06	47 13 30.0	J132937.1+471330	33.6±7.2	20.2±5.8	13.5±5.0	<19.0	<13.2	<10.1	22.8±6.1	13.6±3.7	<16.8
5	13 29 38.01	47 16 13.4	J132938.0+471613	44.7±8.0	39.9±7.5	<11.1	8.9±3.0	8.9±3.0	<4.5	36.1±7.3	30.9±6.8	<11.5
6	13 29 38.63	47 13 36.2	J132938.6+471336	92±11	82.0±9.1	<17.8	20.1±5.7	19.2±5.6	<4.6	71.8±9.8	63.1±9.1	8.8±4.5
7	13 29 42.18	47 14 48.1	J132942.2+471448	28.3±6.6	16.2±5.2	12.1±4.7	8.8±3.0	5.9±2.4	<7.4	19.9±5.7	10.2±4.4	<17.2
8	13 29 43.36	47 15 25.3	J132943.4+471525	133±13	110±12	22.8±6.2	32.0±6.9	26.2±6.3	<12.4	101±11	84±10	17.0±5.5
9	13 29 43.83	47 14 34.6	J132943.8+471435	7.5±2.8	<11.1	<7.9	<10.1	<5.9	<7.6	<9.0	<8.7	<4.1
10	13 29 56.25	47 14 51.6	J132956.3+471452	161±14	119±12	41.8±7.7	<4.0	<4.3	<4.3	162±14	120±12	42.4±7.7
11	13 30 06.47	47 08 34.3	J133006.5+470834	265±16	212±16	53.8±8.5	98±11	78.8±9.9	19.6±5.6	168±14	134±13	34.2±7.0
12	13 30 15.18	47 15 39.0	J133015.2+471539	20.7±6.2	10.3±4.6	<19.5	<12.2	<7.2	<8.6	15.1±5.5	8.0±4.1	7.1±4.3
13	13 30 15.74	47 15 16.5	J133015.7+471517	139±12	118±12	19.8±4.8	21.1±5.9	17.4±5.3	<9.4	116±12	101±11	16.1±4.2
14	13 30 21.01	47 13 53.5	J133021.0+471354	32.9±7.3	29.0±5.6	<10.1	<14.4	<11.4	<6.8	25.8±6.5	23.9±6.1	<7.2
15	13 30 25.11	47 13 13.2	J133025.1+471313	26.3±6.4	18.0±4.4	<16.8	18.7±5.5	12.7±4.8	<12.0	7.6±4.2	<10.3	<8.5
16	13 30 28.45	47 15 20.3	J133028.5+471520	17.7±5.9	14.2±5.2	<9.3	<4.5	<4.5	<4.5	17.1±5.7	13.2±5.1	<9.7
17	13 30 29.34	47 14 28.2	J133029.3+471428	19.1±6.0	13.9±3.9	<12.1	11.8±5.0	<13.5	<11.5	7.3±4.1	6.6±2.6	<4.2

TABLE 5  
ROSAT SOURCE ID

CXO Name (1)	ROSAT Source Name (2)
NGC 5194:	
132939.5+471244 (5), 132940.0+471237 (6)	E4, RW1, M7, IXO78, R1
132943.3+471135 (9)	E5, RW2, M6, IXO79, R2
132945.9+471056 (16)	M5, R3
132946.1+471042 (17)	E6, RW3
...	E7, M4, R4
132950.8+471031 (27), 132951.4+471032 (28)	E8
132953.7+471436 (41), 132953.8+471432 (42)	E10, RW5, M8, R6
133001.0+471344 (69), 133001.1+471333 (70)	E12, RW7, M1, IXO80, R8
133004.3+471321 (76)	M2
133007.6+471106 (82)	E14, RW9, M3, IXO81, R9
Nuclear region	E9, RW4, R5
NGC 5195:	
132959.5+471559 (NGC 5195 - 7)	E11, RW6, R7
133006.0+471542 (NGC 5195 - 12)	E13, NGC 5195 RW1
133006.5+470834 (outside NGC 5194/95)	RW8
Outside <i>Chandra</i> FOV	E1, E2, E3, E15, E16

Note. — Col. (1): *Chandra* name CXOM51 J. The source numbers in Tables 2 and 3 are shown in the parentheses. Col. (2): *ROSAT* source name. E, M, RW, IXO, and R denote the sources in Ehle et al. (1995), Marston et al. (1995), Roberts & Warwick (2000), Colbert & Ptak (2002), and Read, Ponman, & Strickland (1997), respectively.

TABLE 6  
SPECTRAL MODELS OF ULTRALUMINOUS SOURCES ( $L_{0.5-8\text{keV}} > 10^{39}$  ERGS  $\text{s}^{-1}$ )

CXO Name CXOM51 (1)	No. (2)	$N_{\text{H}}$ ( $10^{22}$ $\text{cm}^{-2}$ ) (3)	Photon Index $\Gamma$ (4)	$kT_{\text{in}}$ (MCD) (keV) (5)	$\chi^2/\text{dof}$ (Power law) (6)	$\chi^2/\text{dof}$ (MCD) (7)	Flux (0.5–8 keV) (8)	Luminosity (0.5–8 keV) (9)
NGC 5194:								
J132939.5+471244 (1)	5	0.18 (0.074-0.29)	1.37 (1.09-1.76)	...	11.8/12	...	1.61	1.52
		0.099 (0.030-0.20)	...	1.58 (1.11-2.70)	...	10.6/12	1.27	1.15
J132939.5+471244 (2)	5	0 (<0.087)	1.22 (0.98-1.49)	...	11.4/8	...	0.63	0.54
		0 (<0.043)	...	1.37 (0.98-2.16)	...	11.9/9	0.44	0.38
J132943.3+471135 (1)	9	0.7	10	...	20.4/10	...	...	...
		0.40 (0.25–0.50)	...	0.084 (0.079-0.090)	...	7.0/9	0.27	2.74
J132943.3+471135 (2)	9	0.6	8.2	...	40.0/14	...	...	...
		0.20 (0.13–0.38)	...	0.12 (0.096-0.14)	...	20.5/14	0.21	0.62
J132950.7+471155 (1)	26	5.8 (0.99-12.7)	1.75 (0.73-3.85)	...	3.2/3	...	1.85	2.95
J132950.7+471155 (2)	26	3.6 (2.9-5.6)	1.55 (0.95-2.41)	...	12.2/14	...	2.32	3.95
J132953.3+471042 (2)	37	0.11 (0.060-0.15)	1.55 (1.40-1.74)	...	25.0/33	...	1.58	1.47
		0 (<0.023)	...	1.76 (1.39-2.05)	...	35.9/33	1.49	1.26
J132953.7+471436 (1)	41	0.11 (<0.18)	1.50 (1.28-1.88)	...	6.8/11	...	1.21	1.13
		0.018 (<0.11)	...	1.43 (1.03-2.10)	...	5.5/11	0.98	0.84
J132953.7+471436 (2)	41	0.090 (0.033-0.14)	1.32 (1.15-1.49)	...	27.1/23	...	1.26	1.13
		0.0012 (<0.042)	...	2.20 (1.71-2.84)	...	26.6/23	1.20	1.02
J133001.0+471344 (1)	69	0.12 (0.062-0.15)	1.24 (1.07-1.36)	...	34.9/28	...	2.99	2.71
		0.034 (<0.073)	...	2.34 (1.81-3.31)	...	37.0/28	2.79	2.40
J133001.0+471344 (2)	69	1.6 (0.70-2.0)	9.4 (> 5.1)	...	3.6/6 <sup>a</sup>	...	0.04	57
		0.82 (0.32-1.6)	...	0.17 (0.11-0.30)	...	3.3/6 <sup>a</sup>	0.04	0.56
J133007.6+471106 (1)	82	0.16 (0.11-0.21)	2.26 (2.05-2.50)	...	52.7/47	...	2.85	3.14
		0 (<0.021)	...	0.87 (0.78-0.96)	...	60.5/47	2.46	2.08
J133007.6+471106 (2)	82	0.097 (0.056-2.0)	1.86 (1.69-2.05)	...	66.0/47	...	1.88	1.80
		0	...	1.11	...	91.9/47	...	...
NGC 5195:								
J133006.0+471542 (1)	12	0.10 (<0.19)	1.42 (1.22-1.82)	...	17.3/11	...	1.10	1.01
		0 (<0.092)	...	1.54 (1.11-2.27)	...	14.9/11	0.91	0.79
J133006.0+471542 (2)	12	0.11 (0.046-0.17)	1.32 (1.11-1.51)	...	19.9/19	...	1.20	1.09
		0.039 (<0.086)	...	1.78 (1.32-2.64)	...	19.0/19	1.01	0.87
J132958.4+471547 (2)	5	1.0	10	...	22.7/11	...	...	...
		0.80 (0.18-1.01)	...	0.102 (0.058-0.227)	...	8.9/5	0.062	2.74

Note. — Col. (1): CXO Name (CXOM51). (1) and (2) denote the first (June 2000) and second (June 2001) observation, respectively. Col. (2): Source number in Table 2 (NGC 5194, upper part of Table) and Table 3 (NGC 5195, lower part of Table). Col. (3): Absorbing column density. Col. (4): Photon index for power-law model. Col. (5): Inner disk temperature ( $kT_{\text{in}}$ ) for multi-color disk model. Col. (6):  $\chi^2/\text{dof}$  for power law model. Col. (7):  $\chi^2/\text{dof}$  for MCD model. Col. (8): Observed flux (not corrected for absorption) in the 0.5–8 keV band in units of  $10^{-13}$  erg  $\text{s}^{-1}$   $\text{cm}^{-2}$ . Col. (9): Luminosity (corrected for absorption) in the 0.5–8 keV band in units of  $10^{39}$  erg  $\text{s}^{-1}$ . (a) C-statistic.

TABLE 7  
SPECTRAL MODELS OF SOURCES WITH  $L_{0.5-8\text{keV}} < 10^{39}$  ERGS  $\text{s}^{-1}$

CXO Name CXOM51 (1)	No. (2)	$N_{\text{H}}$ ( $10^{22}$ $\text{cm}^{-2}$ ) (3)	Photon Index $\Gamma$ (4)	$kT_{\text{in}}$ (MCD) (keV) (5)	$\chi^2/\text{dof}$ (Power law) (6)	$\chi^2/\text{dof}$ (MCD) (7)	Flux (0.5–8 keV) (8)	Luminosity (0.5–8 keV) (9)
NGC 5194:								
J132940.0+471237 (1)	6	0.41 (0.26-0.62)	4.47 (3.49-5.88)	...	11.6/13	...	0.48	1.96
		0.14 (0.051-0.23)	...	0.30 (0.24-0.41)	...	13.7/13	0.43	0.59
J132949.0+471053 (2)	21	0.057 (<0.16)	1.26 (0.80-1.69)	...	3.8/5	...	0.47	0.42
		0 (<0.13)	...	1.75 (1.02-4.38)	...	4.2/5	0.38	0.32
J132950.8+471031 (1)	27	0.50 (0.27-0.99)	3.6 (2.6-6.2)	...	1.3/3	...	0.18	0.58
		0.22 (<0.54)	...	0.43 (0.25-0.97)	...	1.6/3	0.15	0.21
J132951.4+471032 (2)	28	0.19 (0.069-0.31)	1.44 (1.13-1.83)	...	3.4/7	...	0.54	0.52
		0.086 (<0.21)	...	1.72 (1.19-2.85)	...	3.1/7	0.47	0.42
J132953.8+471432 (1)	42	0.23 (<0.46)	2.37 (2.00-3.15)	...	1.18/4	...	0.41	0.51
		0 (<0.16)	...	0.90 (0.61-1.20)	...	2.0/4	0.37	0.31
J132953.8+471432 (2)	42	0.17 (0.037-0.30)	1.91 (1.51-2.25)	...	5.8/8	...	0.39	0.40
		0 (<0.14)	...	1.02 (0.64-1.71)	...	9.0/7	0.30	0.26
J132957.6+471048 (1)	63	0.24 (0.061-0.42)	1.88 (1.49-2.48)	...	4.6/5	...	0.57	0.62
		0.10 (<0.24)	...	1.06 (0.71-1.96)	...	4.8/5	0.45	0.42
J132957.6+471048 (2)	63	0.26 (0.15-0.36)	2.13 (1.82-2.53)	...	11.0/15	...	0.64	0.76
		0.094 (0.029-0.17)	...	0.91 (0.72-1.28)	...	10.0/15	0.52	0.49
J132957.6+471206 (1)	64	0 (<0.40)	0.98 (0.36-2.82)	...	0.83/2	...	0.91	0.77
		0 (<0.27)	...	1.93	...	0.85/2	0.63	0.53
J133004.3+471321 (2)	76	0 (<0.16)	1.19 (0.84-1.64)	...	7.0/4	...	0.37	0.32
		0	...	1.86	...	8.8/4	...	...
NGC 5195:								
J132952.8+471644 (2)	1	0 (<0.14)	1.03 (0.68-1.45)	...	4.2/3	...	0.37	0.31
		0 (<0.11)	...	2.36 (>1.51)	...	5.3/3	...	...
J132957.5+471612 (1)	4	0.0058 (<0.33)	1.00 (0.68-1.62)	...	0.40/4	...	0.71	0.60
		0 (<0.11)	...	2.70 (>1.58)	...	0.74/4	0.63	0.54
J132957.5+471612 (2)	4	0.50 (0.27-0.79)	1.85 (1.37-2.81)	...	13.4/8	...	0.48	0.59
		0.25 (0.055-0.59)	...	1.31 (0.83-2.56)	...	13.3/8	0.40	0.41
J132958.7+471625 (2)	6	0.41 (0.051-0.81)	3.3 (2.6-5.1)	...	3.8/4	...	0.14	0.34
		0.14 (<0.48)	...	0.50 (0.33-0.84)	...	3.4/4	0.13	0.14
J132959.5+471559 (1)	7	0 (<0.087)	1.43 (1.18-1.75)	...	13.6/14	...	0.88	0.74
		0 (<0.041)	...	1.59 (1.13-2.34)	...	19.0/14	0.77	0.66
J132959.5+471559 (2)	7	0.11(0.234-0.19)	1.80 (1.58-2.06)	...	25.0/19	...	0.64	0.80
		0 (<0.047)	...	1.22 (1.01-1.45)	...	26.9/19	0.74	0.63
J133003.8+471611 (2)	11	0.43 (0.003-1.1)	3.3 (1.7-6.3)	...	3.2/3	...	0.13	0.31
		0.20 (<0.67)	...	0.45 (0.26-1.04)	...	2.78/3	0.10	0.13
Outside NGC 5194/5195: <sup>a</sup>								
J132943.4+471525 (2)	8	0.099 (< 0.23)	2.02 (1.19-3.43)	...	0.76/3	...	0.22	...
		0 (<0.16)	...	0.74 (0.45-1.17)	...	0.69/3	0.15	...
J132956.3+471452 (2)	10	0.17 (<0.29)	1.87 (1.25-2.23)	...	2.3/7	...	0.44	...
		0 (<0.16)	...	1.25 (0.81-1.65)	...	3.0/7	0.39	...
J133006.5+470834 (1)	11	0 (<0.17)	1.75 (1.41-2.43)	...	2.18/3	...	0.43	...
		0 (<0.099)	...	1.00 (0.69-1.40)	...	4.4/3	0.34	...
J133006.5+470834 (2)	11	0.17 (0.028-0.28)	1.88 (1.57-2.43)	...	8.5/8	...	0.42	...
		0.0071 (<0.11)	...	1.22 (0.88-1.61)	...	8.3/8	0.37	...
J133015.7+471517 (2)	13	0.14	2.2	...	14.1/6	...	0.21	...
		0.009	...	0.75	...	12.7/6	0.17	...

Note. — Col. (1): CXO Name (CXOM51). (1) and (2) denote the first (June 2000) and second (June 2001) observation, respectively. Col. (2): Source number in Table 2 (NGC 5194, upper part of Table), Table 3 (NGC 5195, middle part of Table), and Table 4 (spatially outside NGC 5194 and NGC 5195, bottom part of Table). Col. (3): Absorbing column density. Col. (4): Photon index for power-law model. Col. (5): Inner disk temperature ( $kT_{\text{in}}$ ) for multi-color disk model. Col. (6):  $\chi^2/\text{dof}$  for a power law model. Col. (7):  $\chi^2/\text{dof}$  for a MCD model. Col. (8): Observed flux (not corrected for absorption) in the 0.5–8 keV band in units of  $10^{-13}$  erg  $\text{s}^{-1}$   $\text{cm}^{-2}$ . Col. (9): Luminosity (corrected for absorption) in the 0.5–8 keV band in units of  $10^{39}$  erg  $\text{s}^{-1}$ . (a) Luminosities are  $< 10^{39}$  erg  $\text{s}^{-1}$  if these sources are associated with M51.

TABLE 8  
SPECTRAL MODELS OF NGC 5194 #26

Photon index <sup>a</sup>	$N_{\text{H}}$ ( $10^{22}$ cm <sup>-2</sup> )	Gaussians <sup>b</sup> Energy (keV)	EW (eV)	Suggested ID
Observation 1: 1.55 (1.41-1.70)	...			
...	4.6 (3.8-5.5)			
...	...	1.80 (1.52-1.91)	187 (<507)	Si II – Si XIII K $\alpha$
...	...	3.24 (3.18-3.29)	386 (140-744)	Ar XVIII K $\alpha$ ?
...	...	4.03 (3.96-4.10)	371 (130-694)	Ca XX K $\alpha$
...	...	6.65 (6.50-6.74)	1070 (217-2420)	Fe XX – Fe XXV K $\alpha$
Observation 2: 1.78 (1.38-2.48)	...			
...	0.11 (<0.43)			
...	4.5 (3.5-5.1) (CF <sup>c</sup> 0.988 (0.973-0.995))			

Note. — (a) The photon indices are slightly different from those in Table 6 because, in that table, they are derived assuming a simple power law model without Gaussians and partial covering. (b) Centroid energies of Gaussians are as observed. Lines are assumed to be narrow. (c) Covering factor for partial covering model.

TABLE 9  
SPECTRAL MODELS OF SOFT SOURCES

CXO Name CXOM51 (1)	No. (2)	$N_{\text{H}}$ ( $10^{22}$ cm <sup>-2</sup> ) (3)	$kT$ (keV) (4)	Abundance (solar) (5)	$\chi^2/\text{dof}$ (6)	Flux (0.5-8 keV) (7)	Luminosity (0.5-8 keV) (8)
Blackbody							
J132943.3+471135 (1)	NGC 5194 9	0.26 <sup>+0.39</sup> <sub>-0.24</sub>	0.084 <sup>+0.029</sup> <sub>-0.025</sub>	...	6.7/10	0.27	2.6 (0.79-14)
J132943.3+471135 (2)	NGC 5194 9	0.15 <sup>+0.15</sup> <sub>-0.07</sub>	0.11 $\pm$ 0.02	...	18.5/14	0.12	0.40 (0.26 - 1.0)
J132958.4+471547 (2)	NGC 5195 5	0.67 <sup>+0.60</sup> <sub>-0.66</sub>	0.099 <sup>+0.092</sup> <sub>-0.036</sub>	...	8.9/5	0.062	1.3 (0.056-25)
MEKAL plasma							
J132943.3+471135 (1)	NGC 5194 9	0.44 <sup>+0.24</sup> <sub>-0.15</sub>	0.11 $\pm$ 0.03	< 0.010	8.6/9		
J132943.3+471135 (2)	NGC 5194 9	0.070 <sup>+0.13</sup> <sub>-0.06</sub>	0.24 <sup>+0.04</sup> <sub>-0.06</sub>	0.038 <sup>+0.075</sup> <sub>-0.028</sub>	16.7/13		
J132958.4+471547 (2)	NGC 5195 5	0.97	0.11	0.028	8.5/4		

Note. — Col. (1): CXO name (CXOM51). (1) and (2) denote the first (June 2000) and second (June 2001) observation, respectively. Col. (2): Source name in Table 2 (NGC 5194) and Table 3 (NGC 5195). Col. (3): Absorbing column density. Col. (4):  $kT$  for blackbody or MEKAL model. Col. (5): Abundance for MEKAL model. Col. (6):  $\chi^2 / \text{dof}$ . Col. (7): Observed flux (not corrected for absorption) in the 0.5-8 keV band in unit of  $10^{-13}$  erg s<sup>-1</sup> cm<sup>-2</sup>. Col. (8): Luminosity corrected for absorption in the 0.5-8 keV band in units of  $10^{39}$  erg s<sup>-1</sup>. The range of allowed luminosities is shown in the parentheses.

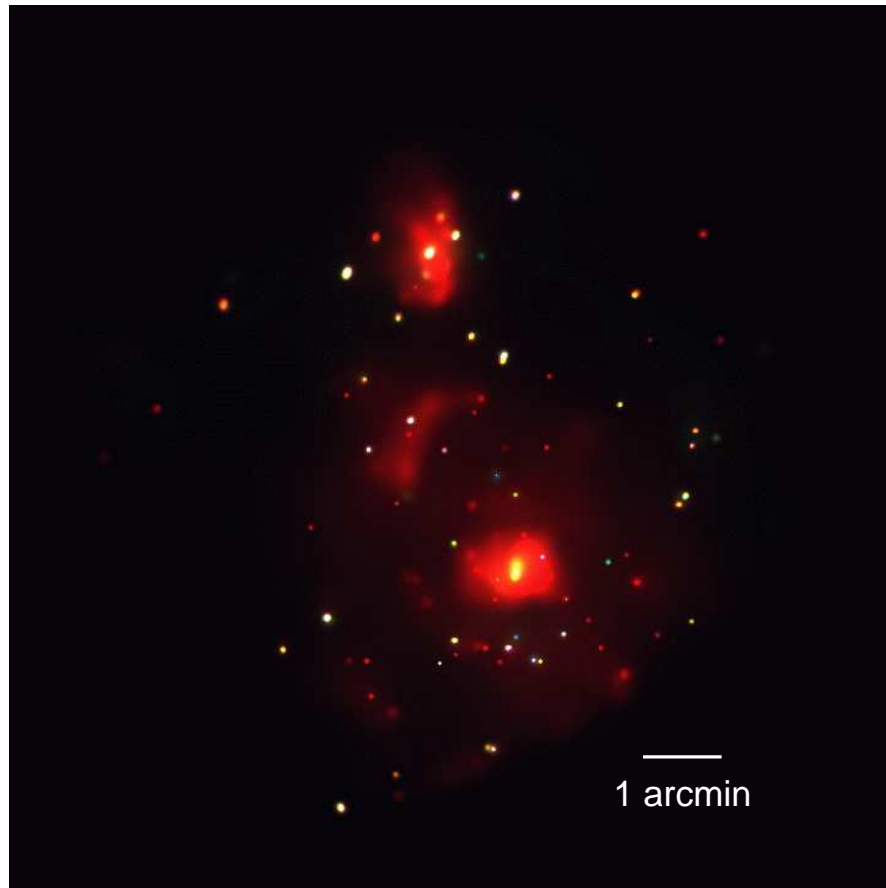


FIG. 1.— Adaptively smoothed color image of M51. Red: 0.3–1.5 keV, Green: 1.5–3 keV, and Blue: 3–8 keV. North is up and East is to the left.

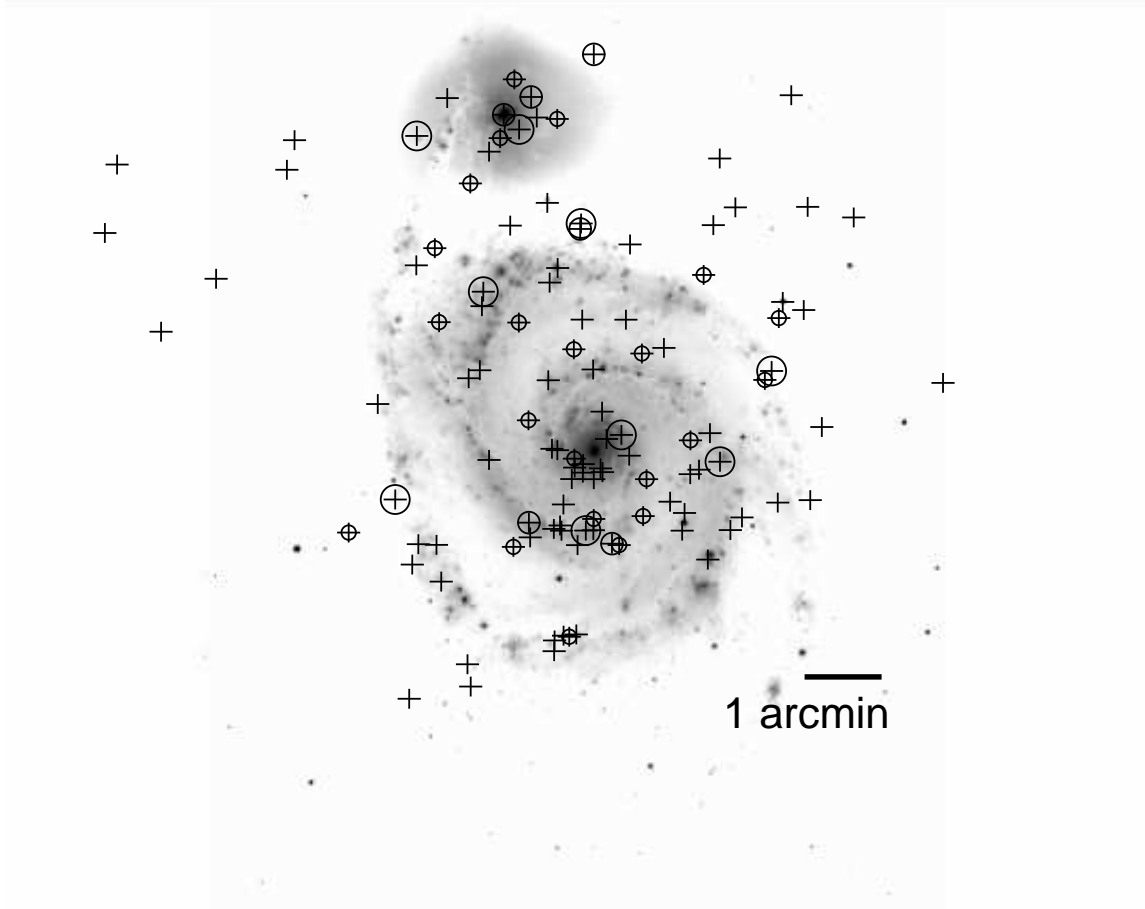


FIG. 2.— X-ray source positions (crosses) overlaid on a narrow band ( $H\alpha$ , continuum not subtracted) optical image (Thilker et al. 2000). Crosses surrounded by large, medium, and small circles correspond to sources with  $L(0.5 - 8 \text{ keV}) > 10^{39} \text{ ergs s}^{-1}$ ,  $L(0.5 - 8 \text{ keV}) = (5 - 10) \times 10^{38} \text{ ergs s}^{-1}$ , and  $L(0.5 - 8 \text{ keV}) = (1 - 5) \times 10^{38} \text{ ergs s}^{-1}$  in the  $0.5 - 8 \text{ keV}$  band, respectively. Crosses without circles correspond to sources with  $L(0.5 - 8 \text{ keV}) \leq 1 \times 10^{38} \text{ ergs s}^{-1}$ . North is up and East is to the left.

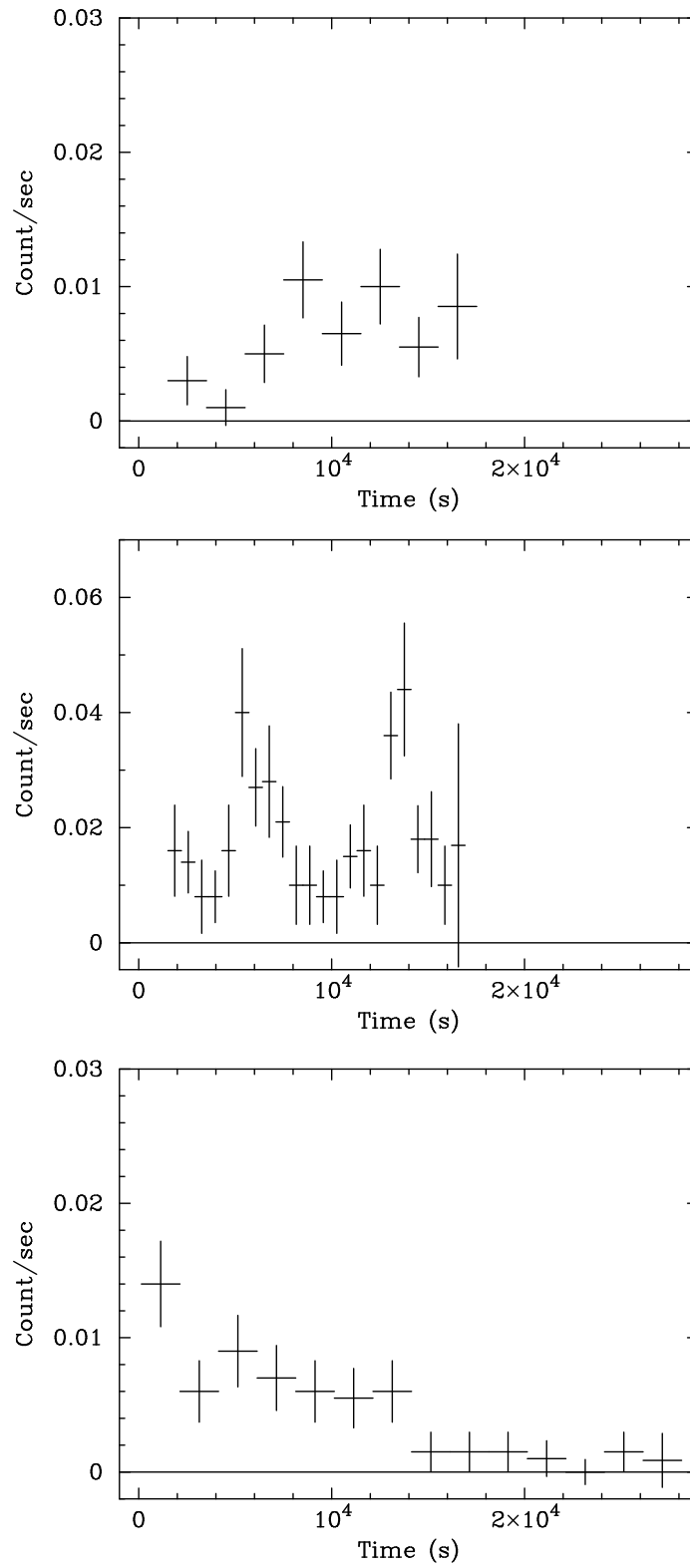


FIG. 3.— Light curves of bright X-ray sources. The background is negligible and has not been subtracted. (a) NGC 5194 #63 = CXOM51 J132957.6+471048 in year 2000 (bin size = 2000 sec), (b) NGC 5194 #69 = CXOM51 J133001.0+471344 in year 2000 (bin size = 700 sec), and (c) NGC 5194 #76 = CXOM51 J133004.3+471321 in year 2001 (bin size = 2000 sec).

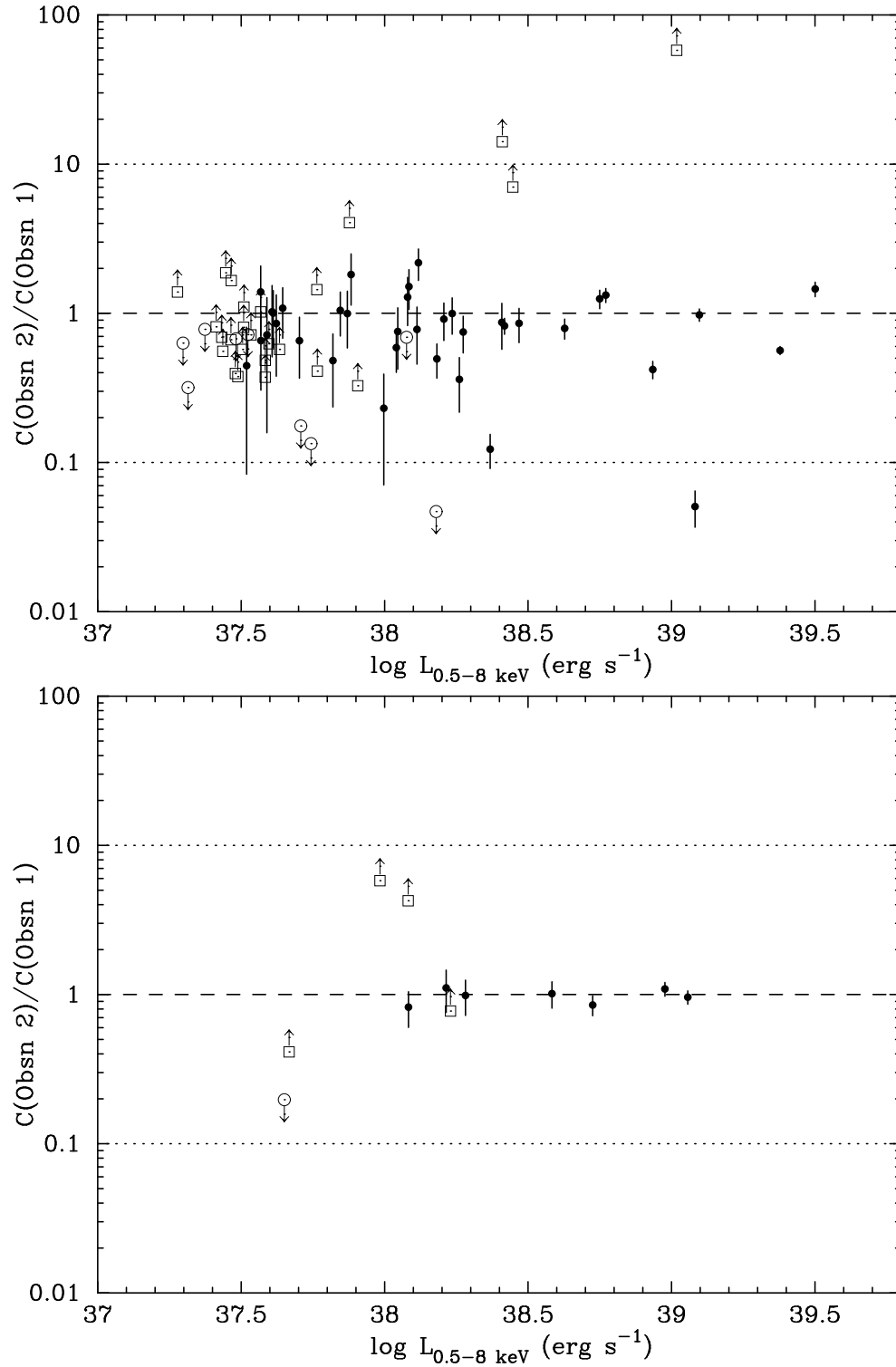


FIG. 4.— Ratios of the count rate (0.5–8 keV band) in the second (June 2001) to that in the first (June 2000) observation as a function of the luminosity in the 0.5–8 keV band. The errors are one-sigma. Upper and lower limits are represented by open circles and open squares, respectively. (a) Sources within NGC 5194. (b) Sources within NGC 5195.

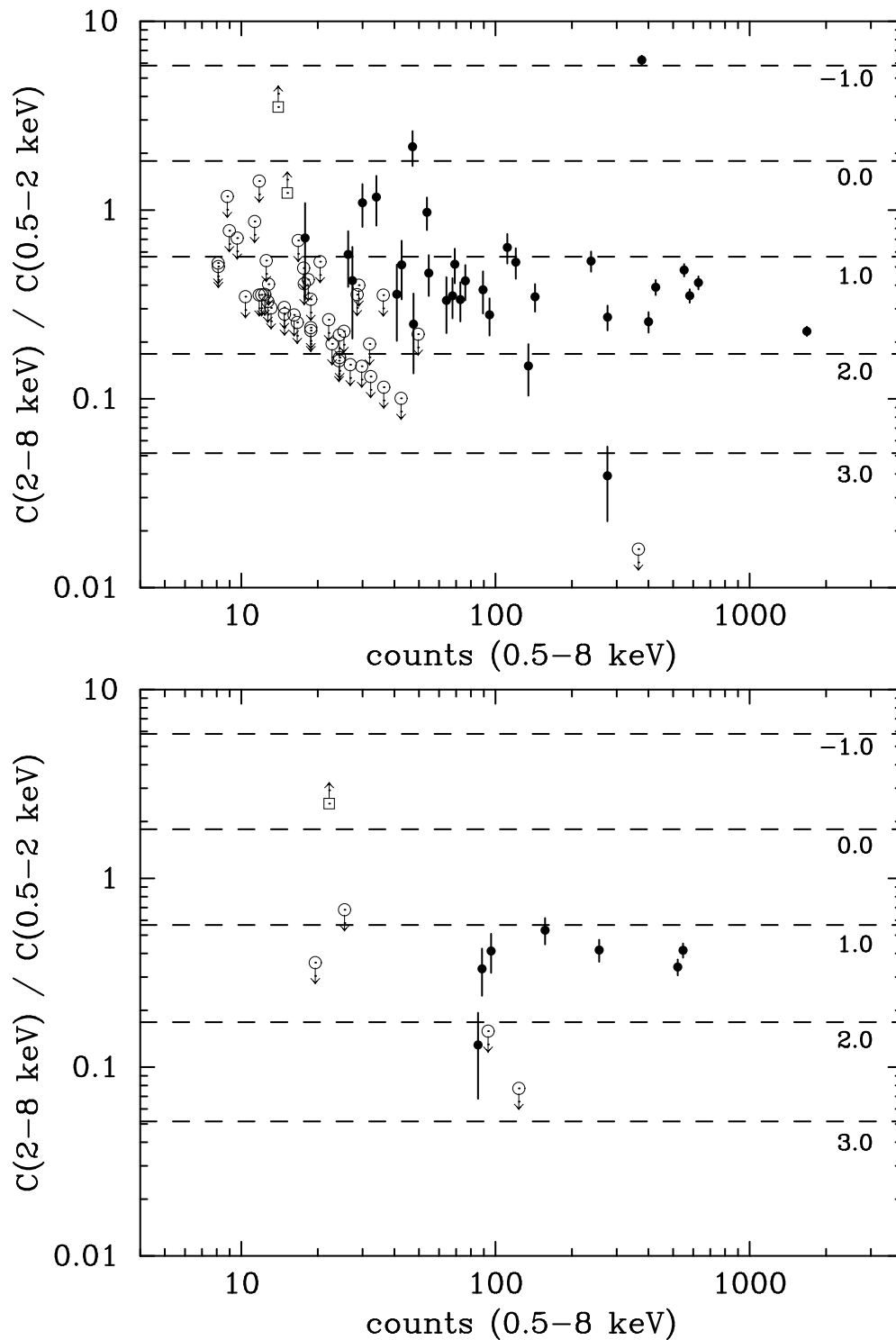


FIG. 5.— Dependence of the band ratio (count rate in 2–8 keV band / count rate in 0.5–2 keV band) on counts in the 0.5–8 keV band for the detected X-ray sources. The horizontal dashed lines correspond to photon indices of  $-1$ ,  $0$ ,  $1$ ,  $2$ , and  $3$  when a power law model absorbed by the Galactic column is assumed. The counts are as observed, and not corrected for the effect of vignetting, and were obtained from the sum of the year 2000 and 2001 observations. (a) Sources within NGC 5194. (b) Sources within NGC 5195.

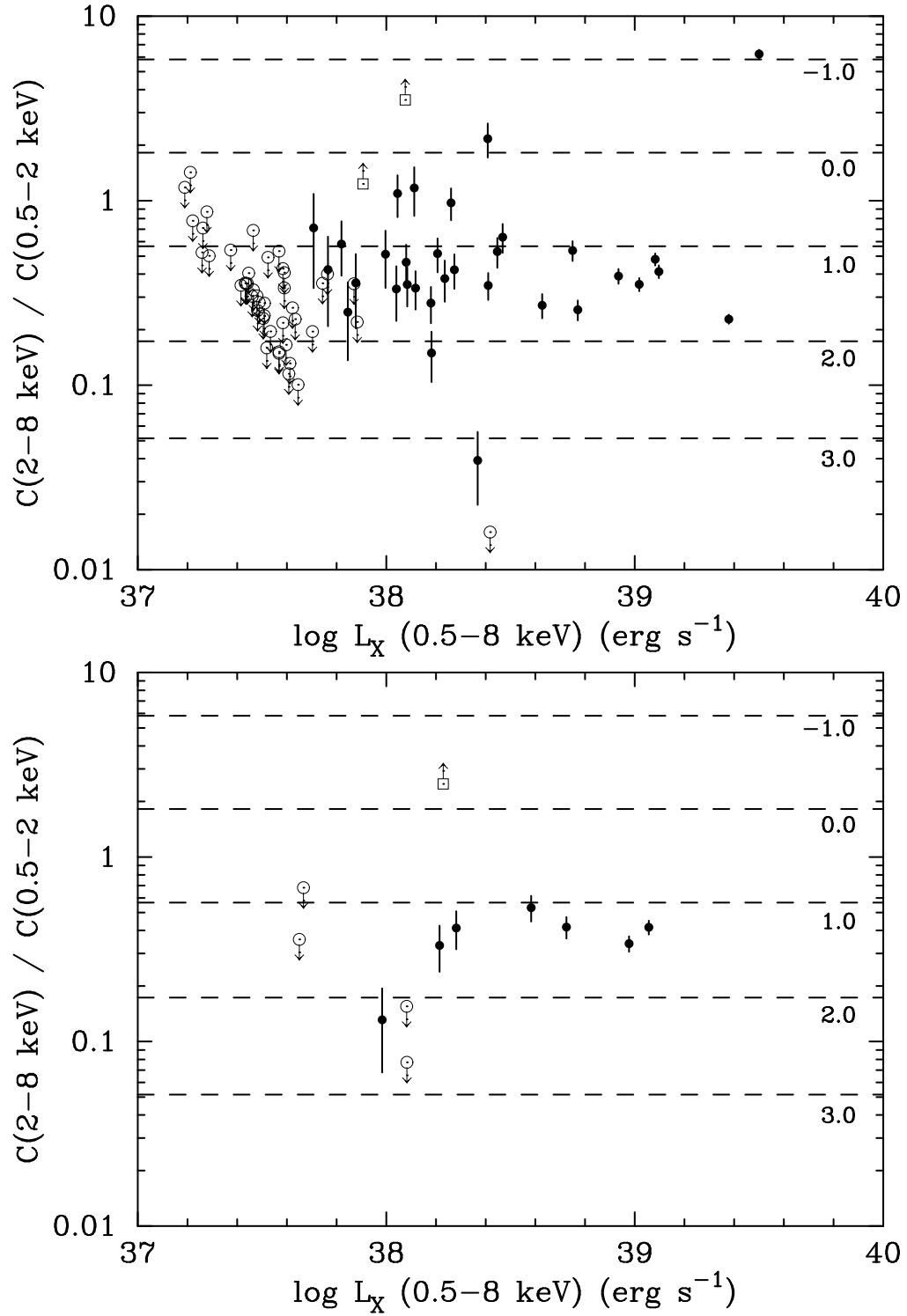


FIG. 6.— Dependence of the band ratio (count rate in 2–8 keV band / count rate in 0.5–2 keV band) on luminosity in the 0.5–8 keV band for the detected X-ray sources. The horizontal dashed lines correspond to photon indices of  $-1$ ,  $0$ ,  $1$ ,  $2$ , and  $3$  when a power law model absorbed by the Galactic column is assumed. The luminosities are corrected for vignetting. (a) Sources within NGC 5194. (b) Sources within NGC 5195.

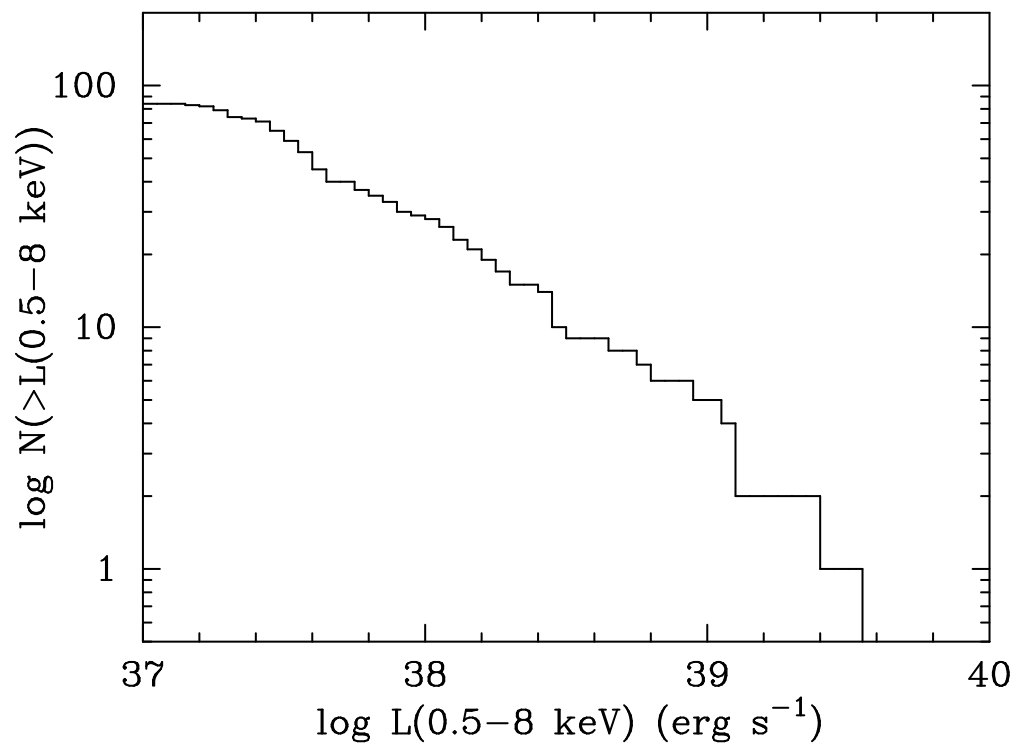


FIG. 7.— Cumulative luminosity function of the X-ray sources in NGC 5194.

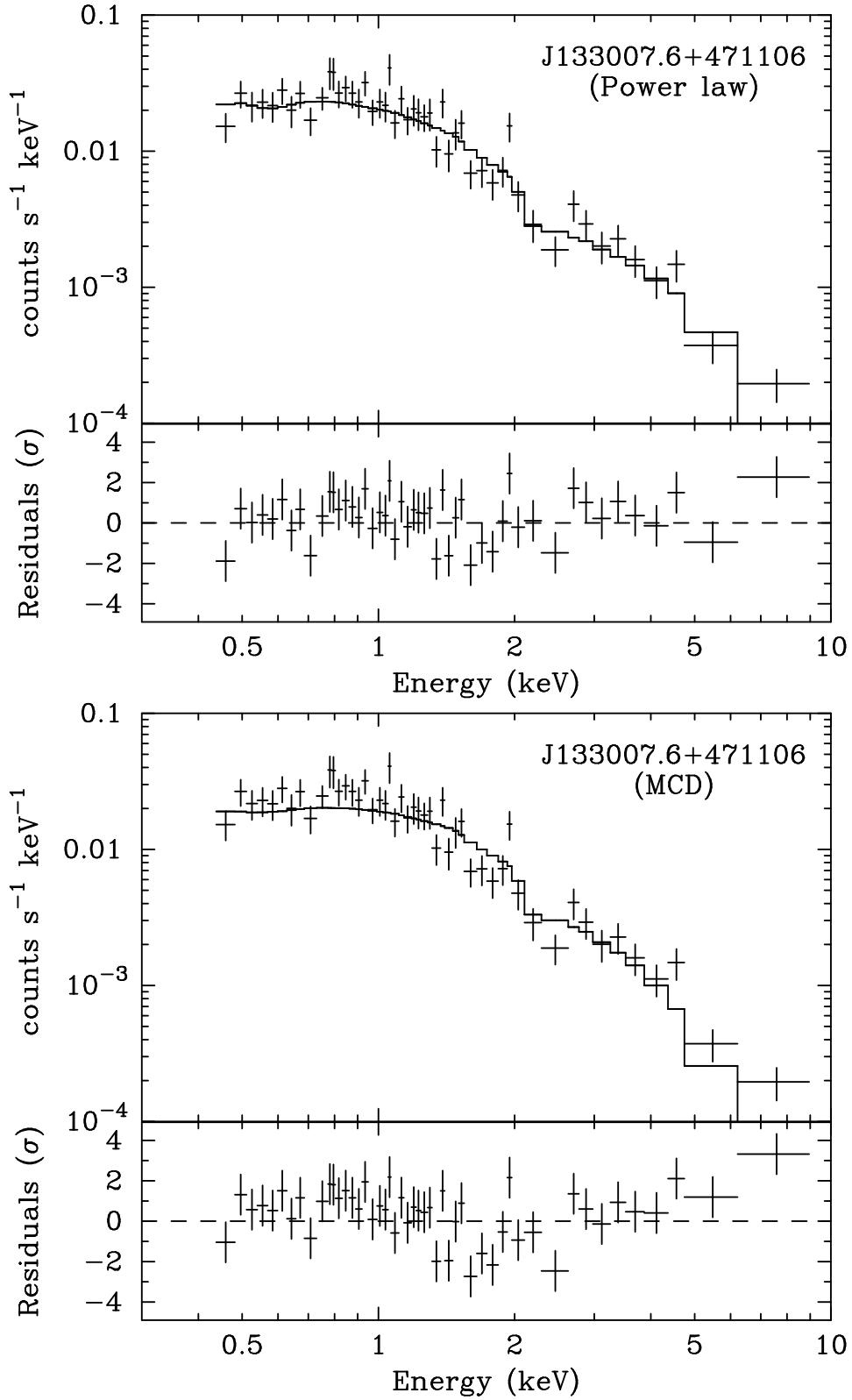


FIG. 8.— X-ray spectrum of NGC 5194 #82 = CXOM51 J133007.6+471106 in 2001 fitted with (a) a power law and (b) a MCD model.

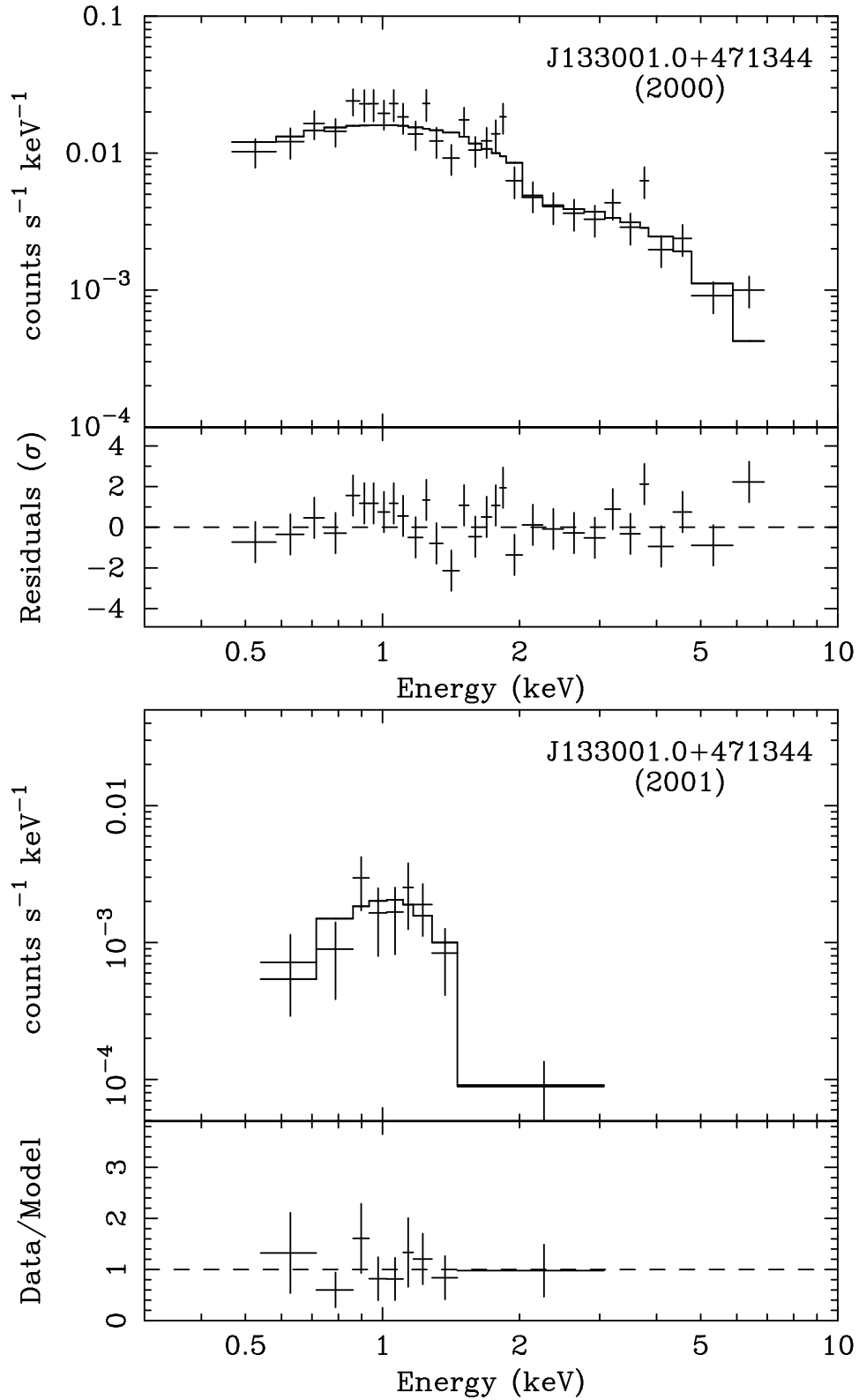


FIG. 9.— X-ray spectra of NGC 5194 #69 = CXOM51 J133001.0+471344. (a) In 2000 fitted with a power law model. (b) In 2001 fitted with a black body model.

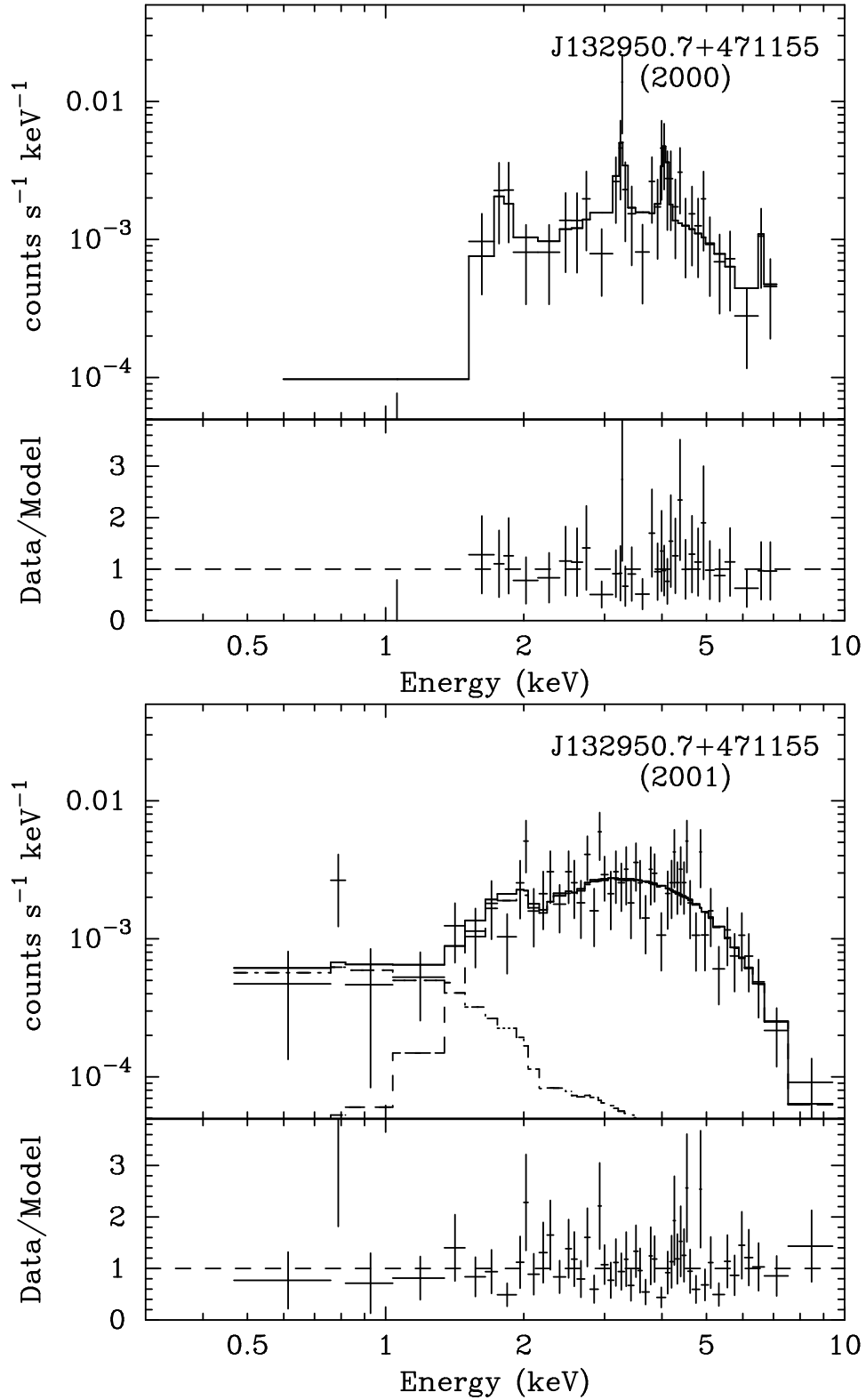


FIG. 10.— X-ray Spectra of NGC 5194 #26 = CXOM51 J132950.7+471155. (a) In 2000 fitted with a power law and four Gaussians (to represent emission lines, see Table 8). (b) In 2001 fitted with a partially covered power law model.

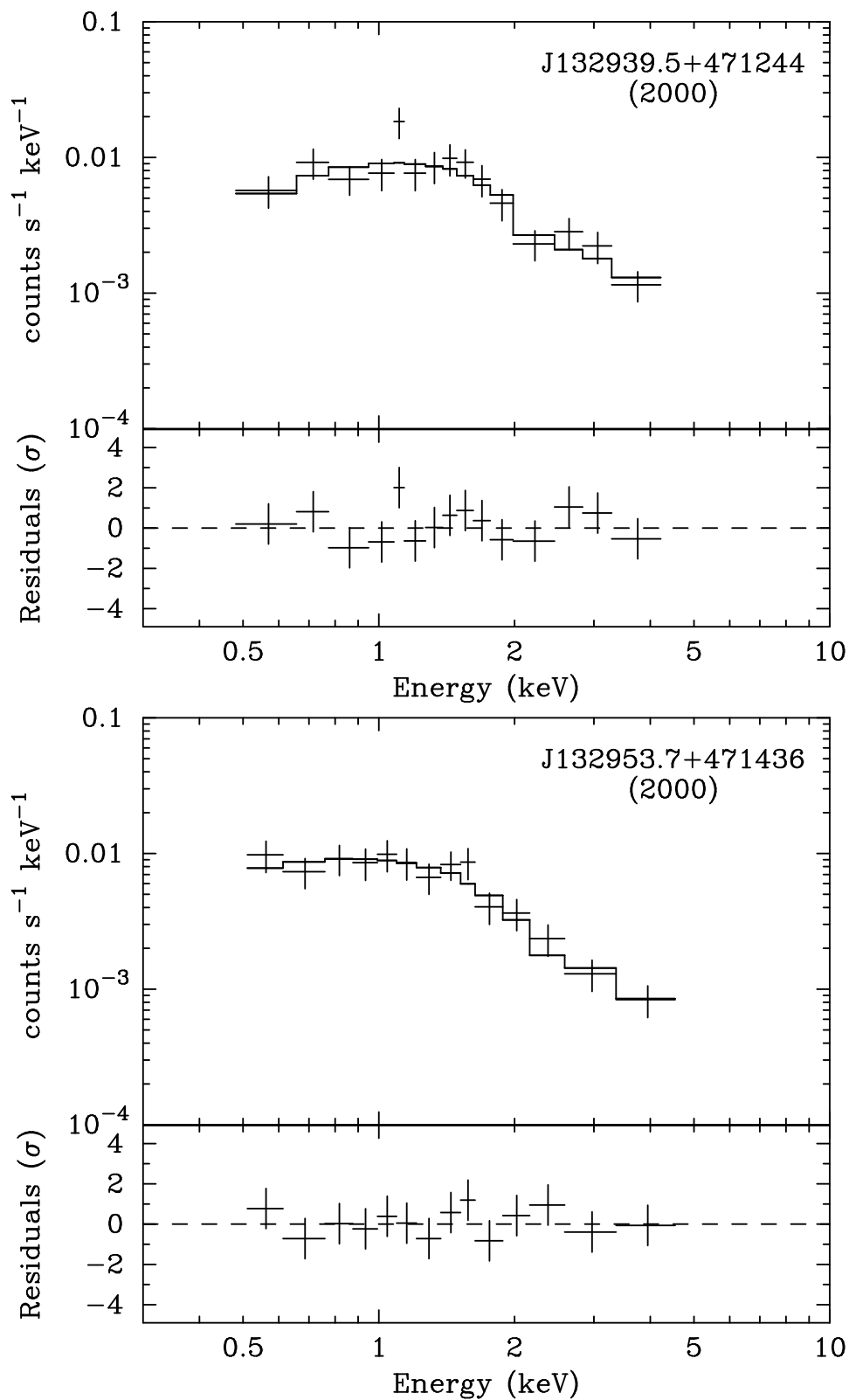


FIG. 11.— X-ray spectra of (a) NGC 5194 #5 = CXOM51 J132939.5+471244 in 2000 and (b) NGC 5194 #41 = CXOM51 J132953.7+471436 in 2000, each fitted with a MCD model.

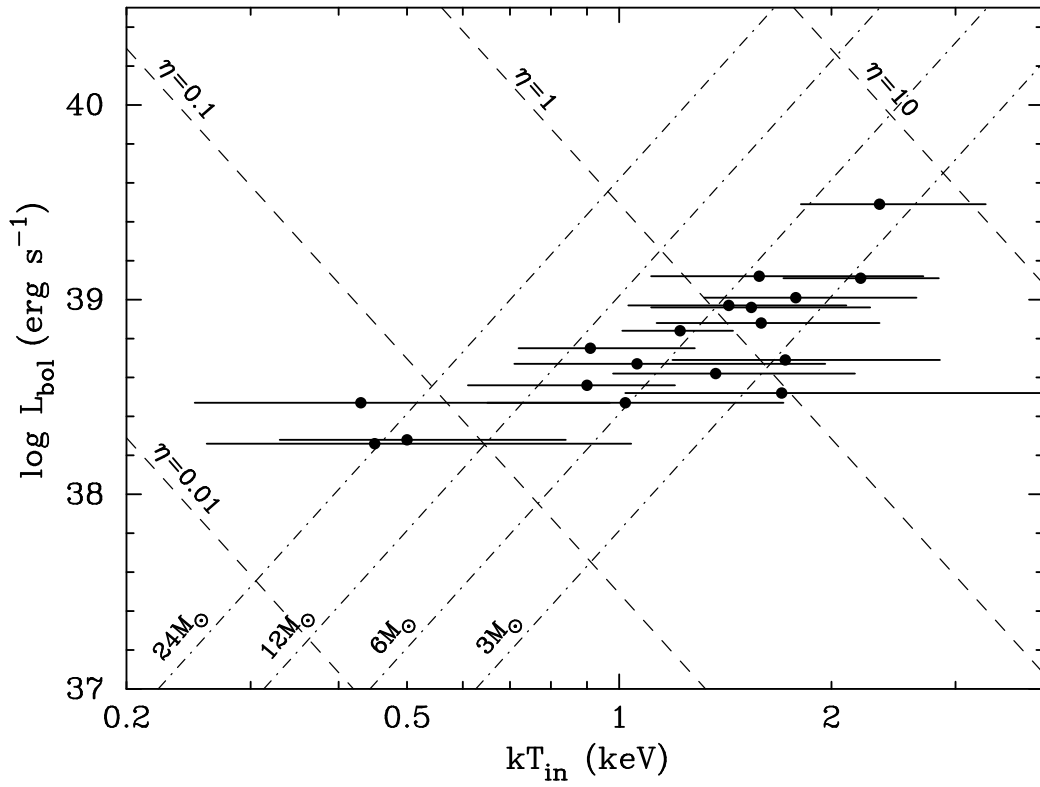


FIG. 12.— The relation between the logarithm of the bolometric luminosity,  $\log L_{\text{bol}}$ , and the inner disk temperature,  $kT_{\text{in}}$  for a thin accretion disk. The expected loci of  $\log L_{\text{bol}}$  and  $kT_{\text{in}}$  for constant black hole masses (3, 6, 12, and  $24 M_{\odot}$ ) and Eddington ratios ( $\eta = 0.01, 0.1, 1,$  and  $10$ ) are shown as the straight dot-dashed and dashed lines, respectively.  $R_{\text{in}} = 3R_{\text{S}}$  is assumed.

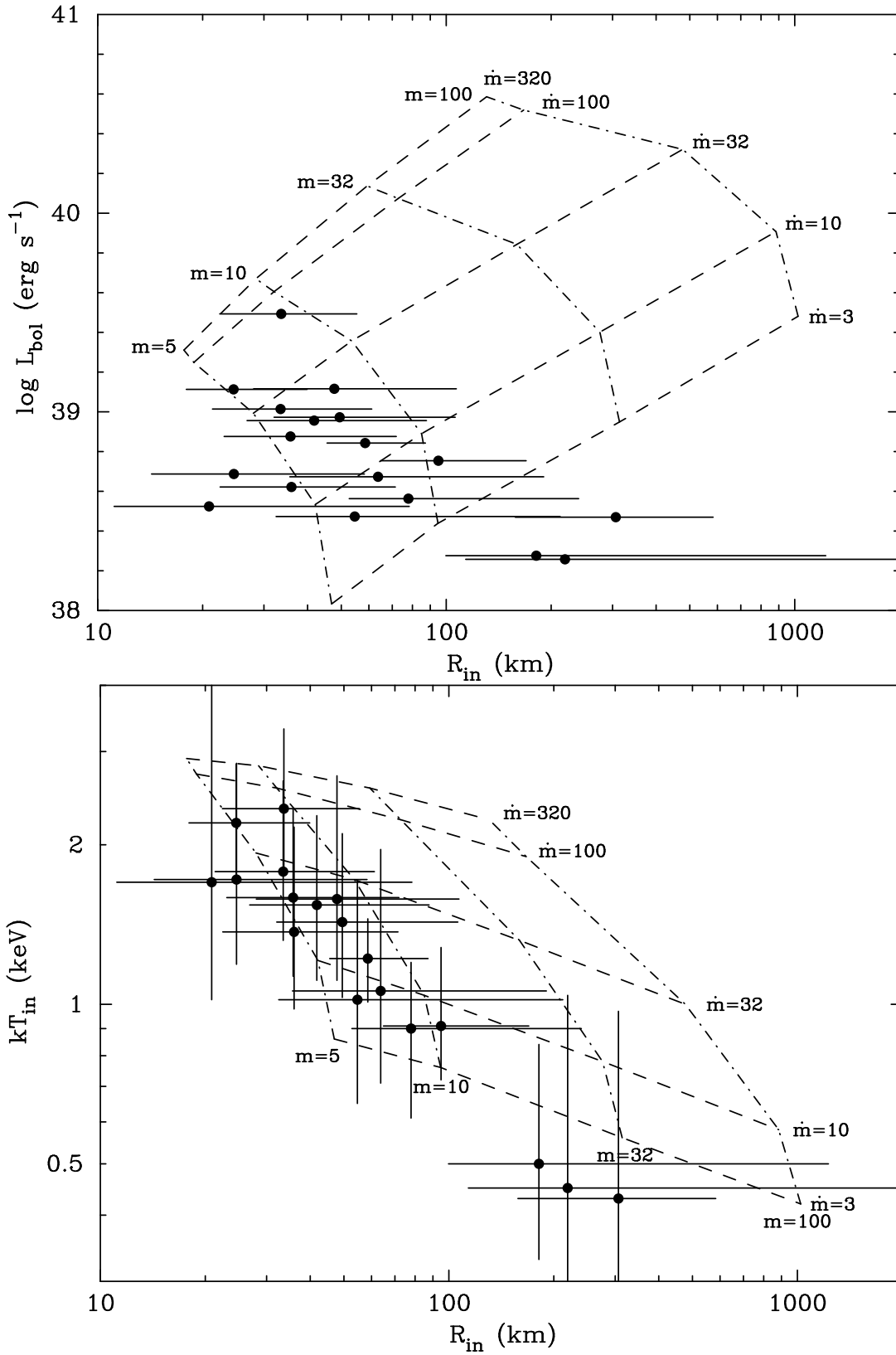


FIG. 13.— Comparison between the MCD parameters inferred from the observations and slim disk model predictions by Watarai et al. (2001). Dash-dotted and dashed lines represent constant  $m = M/M_{\odot}$  and  $\dot{m} = \dot{M}/(L_{Edd}/c^2)$ , respectively. (a)  $\log L_{bol}$ - $R_{in}$  diagram. (b)  $T_{in}$ - $R_{in}$  diagram.

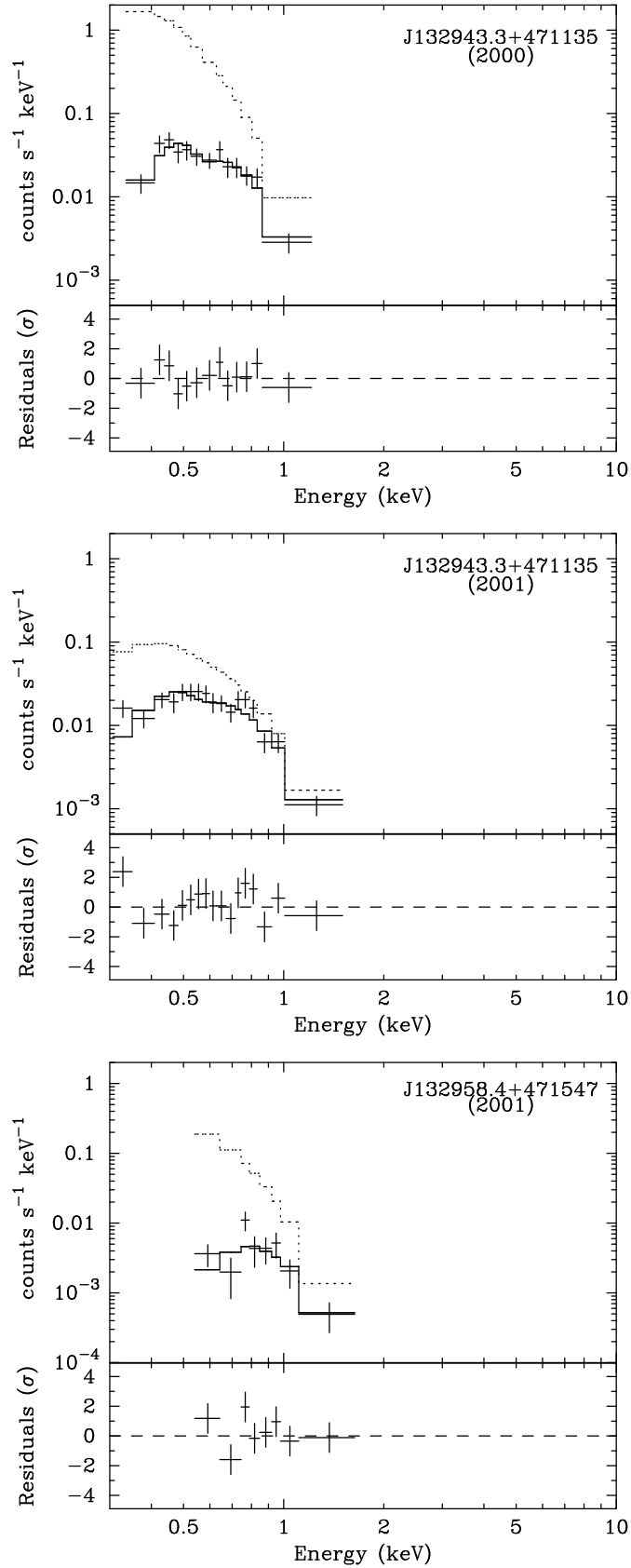


FIG. 14.— Spectra of super soft sources fitted with a black body model. Solid and dotted histograms represent the best-fit model and the model with  $N_{\text{H}}$  set to be zero, respectively. (a) NGC 5194 #9 in the first observation. (b) NGC 5194 #9 in the second observation. (c) NGC 5195 #5 in the second observation.